

Seasonal Evolution of Aleutian Low Pressure Systems: Implications for the North Pacific Subpolar Circulation*

ROBERT S. PICKART,⁺ G. W. K. MOORE,[#] ALISON M. MACDONALD,⁺ IAN A. RENFREW,[@]
JOHN E. WALSH,[&] AND WILLIAM S. KESSLER^{**}

⁺ *Woods Hole Oceanographic Institution, Woods Hole, Massachusetts*

[#] *University of Toronto, Toronto, Ontario, Canada*

[@] *University of East Anglia, Norwich, United Kingdom*

[&] *International Arctic Research Center, Fairbanks, Alaska*

^{**} *NOAA/Pacific Marine Environmental Laboratory, Seattle, Washington*

(Manuscript received 3 August 2007, in final form 15 July 2008)

ABSTRACT

The seasonal change in the development of Aleutian low pressure systems from early fall to early winter is analyzed using a combination of meteorological reanalysis fields, satellite sea surface temperature (SST) data, and satellite wind data. The time period of the study is September–December 2002, although results are shown to be representative of the long-term climatology. Characteristics of the storms were documented as they progressed across the North Pacific, including their path, central pressure, deepening rate, and speed of translation. Clear patterns emerged. Storms tended to deepen in two distinct geographical locations—the Gulf of Alaska in early fall and the western North Pacific in late fall. In the Gulf of Alaska, a quasi-permanent “notch” in the SST distribution is argued to be of significance. The signature of the notch is imprinted in the atmosphere, resulting in a region of enhanced cyclonic potential vorticity in the lower troposphere that is conducive for storm development. Later in the season, as winter approaches and the Sea of Okhotsk becomes partially ice covered and cold, the air emanating from the Asian continent leads to enhanced baroclinicity in the region south of Kamchatka. This corresponds to enhanced storm cyclogenesis in that region. Consequently, there is a seasonal westward migration of the dominant lobe of the Aleutian low. The impact of the wind stress curl pattern resulting from these two regions of storm development on the oceanic circulation is investigated using historical hydrography. It is argued that the seasonal bimodal input of cyclonic vorticity from the wind may be partly responsible for the two distinct North Pacific subarctic gyres.

1. Introduction

The fall and winter atmospheric circulation over the North Pacific Ocean is dominated by a progression of low pressure systems propagating from west to east (Overland and Hiester 1980). These systems originally form off the Asian continent due to the contrast between different air masses: cold, dry air originating from Siberia, and warm, moist maritime air from the subtropical Pacific (Terada and Hanzawa 1984). The low

pressure centers tend to be associated with large-scale upper-level planetary waves (Roden 1970), and they derive their energy via the lower tropospheric temperature gradient, which is influenced by the North Pacific sea surface temperature (SST) front. As these lows progress eastward, they often intensify further in the region of the Aleutian Island chain (Wilson and Overland 1986; Terada and Hanzawa 1984; Zhang et al. 2004) and develop into powerful storms that have a wide area of influence. These systems are commonly referred to as Aleutian lows, and their strength and frequency are the reason why the northeast Pacific is one of the stormiest regions in the World Ocean (Wilson and Overland 1986).

While the primary track of Aleutian lows is from west to east along the subpolar front, there are numerous variations to this basic pattern that occur on time scales

* Pacific Marine Environmental Laboratory Contribution Number 3133.

Corresponding author address: Robert S. Pickart, Clark 3/MS 21, Woods Hole Oceanographic Institution, Woods Hole, MA 02543.
E-mail: rpickart@whoi.edu

from weeks to years. For example, Anderson and Gyakum (1989) identified six different regimes where storm tracks are found in different areas of the western North Pacific and Gulf of Alaska, including one configuration where storms enter directly into the Bering Sea. Storms also occasionally enter the Gulf of Alaska from the south (Terada and Hanzawa 1984; Wilson and Overland 1986). Numerous factors influence the detailed trajectory and ultimate fate of the Aleutian lows. First, the presence of the Siberian high, and a ridge of high pressure that often extends southeastward from it, can prohibit storms from progressing northward (Fig. 1a; see also Overland and Hiester 1980; Wilson and Overland 1986). One consequence of such blocking is that pack ice can form more readily in the Bering Sea, due in part to the absence of warm air otherwise brought northward by the storms (Overland and Pease 1982). Another consequence is that it cuts off one of the primary pathways for cyclones to enter the Arctic domain in the vicinity of the Bering Strait (Zhang et al. 2004). A second type of blocking due to high pressure can occur in the central North Pacific during winter. This pattern (Fig. 1b) diverts eastward-propagating Aleutian lows either to the north or south (Wilson and Overland 1986). In addition to the upper-level steering currents, the orography of the land can influence storm movement and development. In particular, the mountain ranges of coastal Alaska and Canada often impede the passage of storms (Wilson and Overland 1986), causing them to stall and subsequently spin down. Indeed, the eastern Gulf of Alaska is known as the “graveyard” of Pacific storms (Plakhotnik 1964; Gyakum et al. 1989; Rodionov et al. 2005a).

There is both a clear seasonality and a marked interannual variation of the North Pacific storm climate. In an integrated sense (monthly, yearly), the composite signature of the cyclones is represented by the strength and position of the Aleutian low sea level pressure (SLP) signal (analogous to the Icelandic low signal in the North Atlantic). This signal first appears in early fall in the eastern Bering Sea in the vicinity of the central Aleutian Island arc. The signal then deepens significantly, and its center of action moves southeastward into the Gulf of Alaska. Later, during the early winter months, there is a second transition as the low pressure signal moves rapidly to the west and is located in the region southeast of Kamchatka. This seasonal clockwise progression has long been established (e.g., Favorite et al. 1976), and the two resulting areas of enhanced storm activity—in the Gulf of Alaska and in the western North Pacific—are well documented (e.g., Sanders and Gyakum 1980; Terada and Hanzawa 1984; Wilson and Overland 1986; Gyakum et al. 1989; Zhang et al. 2004).

However, the precise reasons for this “bimodality” in the seasonal low pressure signature of the Aleutian low have yet to be clearly established.

On interannual time scales, the Aleutian low varies strongly as well. Trenberth and Hurrell (1994) defined the North Pacific Index (NPI) as the area-weighted sea level pressure over the Bering Sea and part of the North Pacific. While related to the Pacific–North American teleconnection pattern (e.g., Feldstein 2003; Wallace and Gutzler 1981), the NPI is representative of the strength of the wintertime Aleutian low. Trenberth and Hurrell (1994) showed that the NPI varies significantly on long time scales and can go through extended phases lasting a number of years. For instance, the NPI was especially low from 1976 to 1988 (1976 marked the beginning of the well-known regime shift of the North Pacific; Mantua et al. 1997). During this period, the center of action of the NPI shifted eastward, and the tracks of the Aleutian lows were situated more to the south.

Rodionov et al. (2005a) elucidated this by comparing composite averages of low and high NPI periods. Among other things, they demonstrated the importance of the upper-level steering currents in dictating the storm tracks. In particular, during the low NPI periods (strong Aleutian low) the configuration of the “East Asian trough” and “North American Ridge” kept storms at a more southerly latitude in the western and central North Pacific, then diverted them sharply to the northeast into the central Gulf of Alaska. By contrast, during the high NPI periods (weak Aleutian low) the storms were situated farther to the north (with more of them veering into the Bering Sea) and progressed into the eastern Gulf of Alaska. It has been demonstrated that these different configurations have numerous environmental impacts, including variability of sea surface temperature along the coast of Alaska and the west coast of Canada (e.g., Davis 1976) and differences in the severity of winters near the Aleutian Islands (e.g., Rodionov et al. 2005a). Rodionov et al. (2005b) showed that the Aleutian low—both its magnitude and location—strongly influences wintertime air temperatures in the Bering Sea as well (although there was no statistical link to the NPI or other indices related to the Aleutian low).

Using cyclone tracking, Zhang et al. (2004) also found significant interannual changes in the storm activity of the North Pacific, including enhanced storminess during the period 1950 to 1980. This has far-reaching consequences since a number of these storms progress into the Arctic region. Zhang et al. (2004) note that more storms enter the Arctic (in a circumpolar sense) from midlatitudes than are formed locally in the polar domain. Another aspect of interannual variability was described by White and Barnett (1972), who argued that

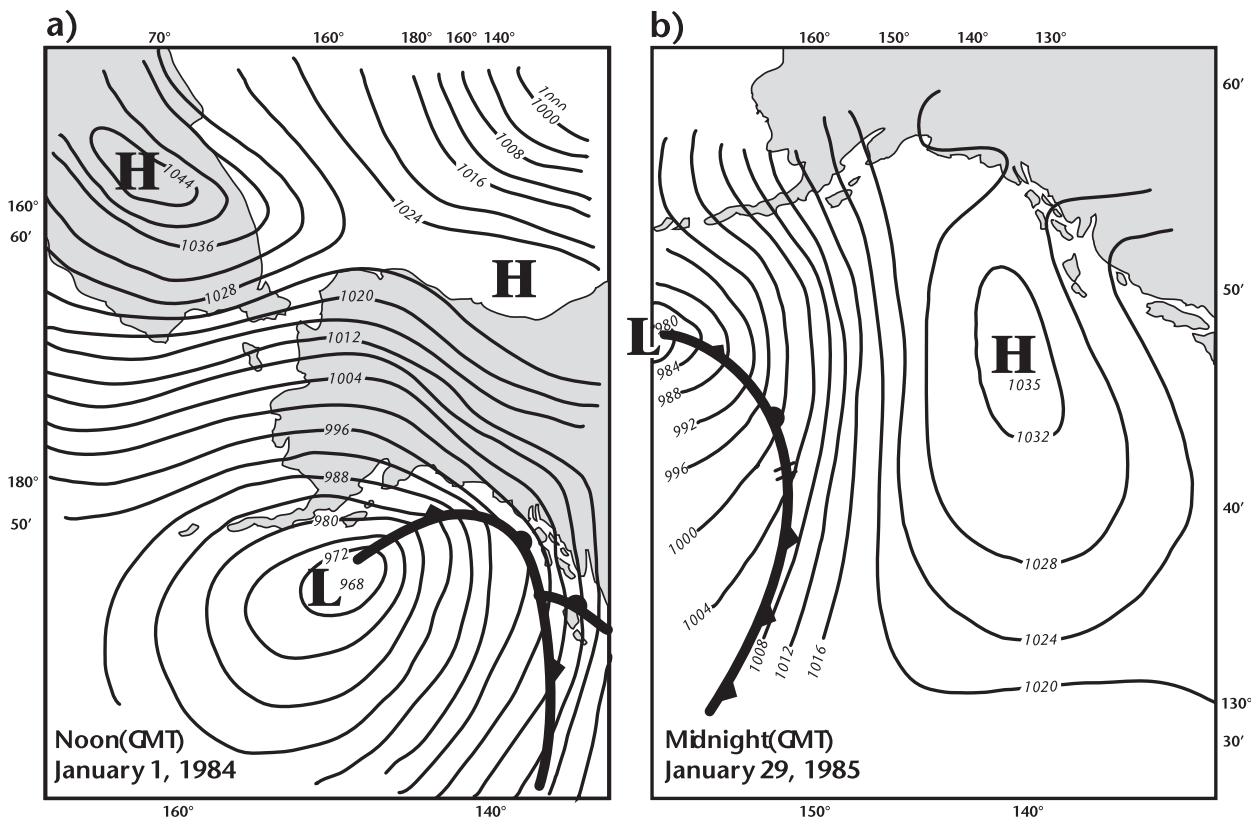


FIG. 1. Typical wintertime atmospheric configurations in the North Pacific (from Wilson and Overland 1986). (a) An Aleutian low pressure system in the Gulf of Alaska and a Siberian high to the northwest, with an associated ridge of high pressure extending to the east. (b) An Aleutian low impinging on a blocking high situated in the Gulf of Alaska.

the strong upper-level westerly airflow associated with enhanced Aleutian low systems may be barotropically unstable. This in turn could drive the system toward a state where there are less frequent low pressure systems and weaker westerly flow aloft, due to the amplification of a quasi-stationary long wave.

It is clear that Aleutian low storms have a wide-ranging influence on many aspects of the North Pacific and western Arctic atmosphere–ocean system, including the subpolar ocean circulation, evolution of pack ice, and northward transport of atmospheric moisture (Smirnov and Moore 2001). Hence, it is important to understand what factors dictate the storm development and evolution, and how these factors might vary through the fall and winter seasons. This is the motivation for the present study. We use a combination of meteorological reanalysis fields, satellite wind and SST data, and historical oceanographic station data to elucidate our understanding of the cyclogenesis of these storms—including the role of the seasonally varying SST field—and how the storms might in turn influence the subpolar ocean circulation. Among other things we offer an explanation for the seasonal progression of the Aleutian

low sea level pressure signal described above, as well as why there are two distinct regions of enhanced storm activity in the North Pacific. We focus primarily on a single year, the fall–winter of 2002, which enables a detailed case study encompassing all of the storms during this period. It is demonstrated, however, that the conclusions reached here are indicative of the canonical seasonal trends associated with Aleutian low storms.

2. Data and methods

We consider the 4-month period from September through December 2002 (though later in the study we consider various climatological averages). The reason for choosing this particular year is that a mooring array was maintained in the southern Arctic Ocean during this time period, and the measured circulation was strongly impacted by the wind field associated with Aleutian low pressure systems. The relationship between the Pacific-born storms and the flow field of the southern Arctic Ocean is addressed in a companion paper (Pickart and Moore 2008, manuscript submitted to *J. Geophys. Res.*). Here, we focus on the evolution of

the storms themselves and the local impact they have on the circulation of the North Pacific Ocean.

a. Sources of data

To analyze the tracks and characteristics of the storms during the 4-month period, the 6-hourly meteorological reanalysis fields from the National Centers for Atmospheric Prediction (NCEP) were used. Prior to the analysis we computed adjusted sensible and latent heat flux fields as employed in Moore and Renfrew (2002). Using a bulk formula following that of Smith (1988) and using the transfer coefficients of DeCosmo et al. (1996), this was applied to the NCEP surface fields. Fluxes computed as such have been shown to be more representative of the actual heat fluxes measured in subpolar regions (see Renfrew et al. 2002). The horizontal resolution of the NCEP sea level pressure data is 2.5° , and the other NCEP fields used in the study are on a Gaussian grid with variable resolution in the north-south direction ($\sim 1.9^\circ$) and 1.875° in the east-west direction. For ease of use, the sea level pressure was interpolated onto the same grid as the other NCEP fields. The SST fields are from the Advanced Very High Resolution Radiometer (AVHRR) and were obtained from the Comprehensive Large Array-Data Stewardship System (CLASS) of the National Oceanic and Atmospheric Administration (NOAA). The resolution of these fields is 100 km.

Later in the study, we use scatterometer wind data from the SeaWinds instrument on the Quick Scatterometer (QuikSCAT) satellite. These are available twice daily from Remote Sensing Systems, Inc. (Wentz et al. 2001), and they have a horizontal resolution of $1/4^\circ$. We also use European Remote Sensing Satellite (ERS) winds that were processed into monthly, 1° gridded fields of stress components by the Centre ERS d'Archivage et de Traitement (CERSAT). The hydrographic analysis was carried out using HydroBase 2 (Curry 2002), which contains an extensive database from the Pacific Ocean. This includes bottle stations and conductivity-temperature-depth (CTD) casts from the World Ocean Database 1998, along with more recent data from the World Ocean Circulation Experiment (WOCE) and many individual cruises. In the present analysis of the North Pacific (confined to south of 60°N because of sparse data coverage farther north), most of the hydrographic data fall within the time period 1940 to 2000. To create the climatological lateral fields, the data were averaged onto 1° grids. One of the advantages of HydroBase 2 is that this averaging is done along density surfaces, which more accurately captures features associated with strong fronts (such as the North Pacific front) than does depth averaging. [For details, the

reader is referred to Curry (2002) and Macdonald et al. (2001).]

b. Storm tracking

Although automated cyclone detection schemes have been used to track storms (e.g., Serreze et al. 1997; Zhang et al. 2004), we chose to perform this task manually, following the methodology of Pickart et al. (2003) and Våge et al. (2008). A disadvantage of this approach is that it is too time consuming to consider multiple years; hence, our sample size of storms is small. Furthermore, all of the storms are given equal weighting. This should be kept in mind when considering the results below. However, a strong advantage of manual tracking is that features will not escape detection, and complex storm events are less apt to be misrepresented. As mentioned above, the North Pacific is one of the stormiest regions of the World Ocean, and often during the fall of 2002 multiple storms were present within the domain. Consequently, storms interacted on a regular basis (e.g., merging events, splitting events) and great care was taken to document such behavior accurately. Another scenario that was not uncommon was for a given storm to have more than one significant deepening event. It should be noted that sometimes subjective decisions were made regarding the evolution of some of the more complex storm systems. By and large, however, the ability to track individual storms, as well as their interactions, was fairly straightforward.

The domain of interest extends from 130°E to 110°W , and 28° to 80°N . Each well-defined cyclone was tracked in this domain from 1 September to 31 December 2002. For each 6-h period, the latitude, longitude, and central sea level pressure of the storm was documented. An example of a representative storm track is shown in Fig. 2a. This particular storm followed a generally west-to-east path, with an excursion to the south near the Aleutian Island arc. For each track we tabulated various features of the storm. First, the primary deepening event of the storm was identified, as well as any secondary deepening events (early in the fall some storms had more than one occurrence of cyclogenesis, as discussed below). The magnitude of the deepening was computed (largest negative rate of change of the central pressure over a 12-h period), and the minimum pressure of the event was documented. Next, the location and central pressure at which the storm filled was determined. The criterion for filling was when the rate of pressure rise approached zero or slowed considerably, which sometimes was determined subjectively. In instances when storms deepened twice, the final filling was used. Sometimes after the filling rate decreased, a storm would suddenly start weakening further, usually as the storm left the domain.

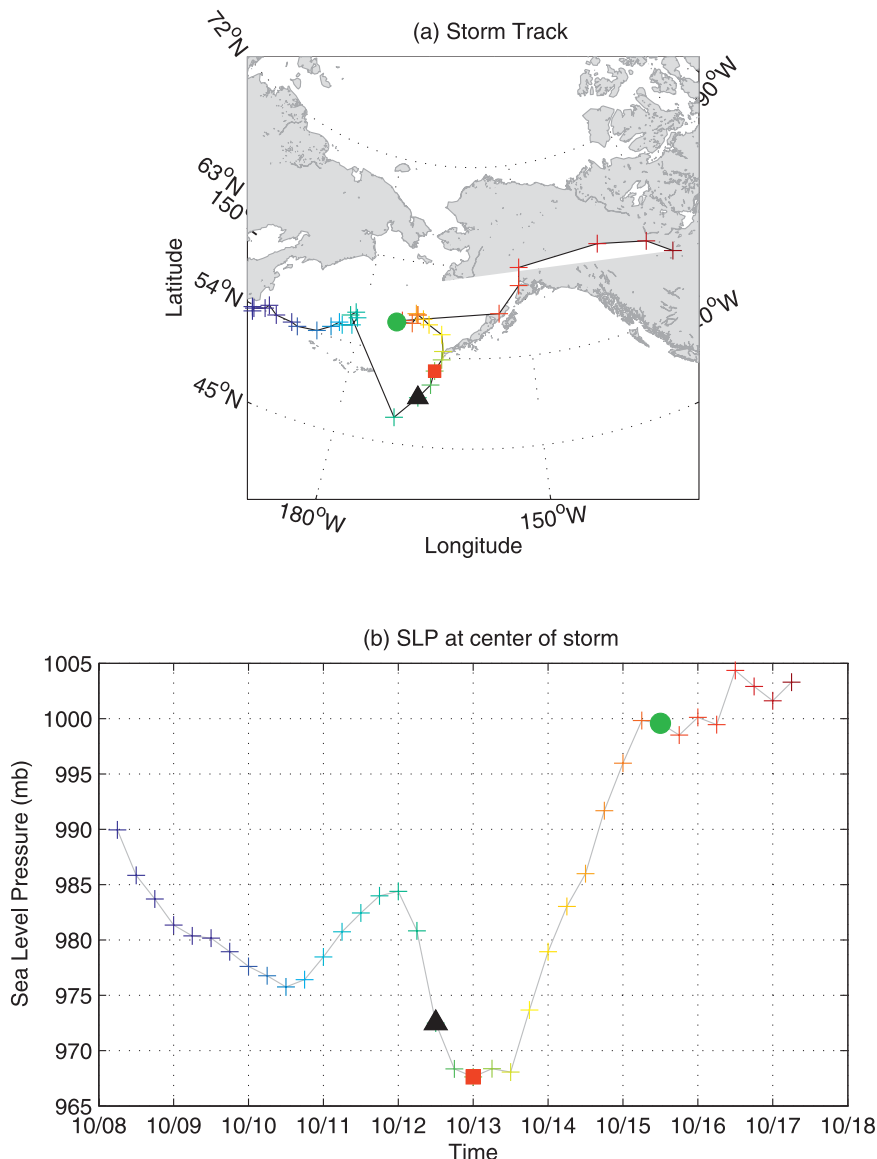


FIG. 2. Example of the storm tracking used in the analysis. (a) Track of an Aleutian low pressure system in October 2002. The plus symbols denote the 6-hourly locations, color coded by time (blue is early October, red is mid-October). The black triangle is where the storm deepened rapidly, the red square is where it obtained its minimum sea level pressure, and the green circle is where the storm filled. (b) Time series of the central sea level pressure following the storm. This shows how the features explained in (a) were defined.

These later parts of the storms were discounted. Finally, the distance that the storm traveled over each 6-h period was computed. For the example in Fig. 2, the maximum deepening, minimum pressure, and filling of the storm are marked by different symbols.

3. Mean fields and storm characteristics

The mean sea level pressure (SLP), surface wind field, and SST for fall 2002 are presented in Fig. 3. The sig-

nature of the Aleutian low dominates the SLP distribution (Fig. 3a). The minimum pressure is located over the Alaska Peninsula, but the area of reduced SLP extends far to the west into the Sea of Okhotsk. The cyclonic wind field associated with the Aleutian low is nicely captured in the QuikSCAT data (Fig. 3b), showing a wide band of strong westerly winds across the basin. Note also the enhanced winds in the narrow region adjacent to the southeast coast of Alaska. These are barrier winds associated with the high topography of the coast

(Loescher et al. 2006). The mean SST field (Fig. 3c) shows the North Pacific front, which extends across the entire basin. Note how the isotherms of the front bend to the north starting around 165°W. We refer to this bend as the “SST notch,” which turns out to be an important feature for the meteorology, as discussed below.¹ The primary reason for the notch is that the northward-flowing Alaska current (the eastern boundary current of the Alaska gyre) carries warm water cyclonically around the Gulf of Alaska (see Figs. 13, 16). Note that this feature is present year-round (while the Aleutian low SLP signal is absent in the summer months).

Despite the smoothly varying mean SLP pattern in Fig. 3a, the region was characterized by many powerful storms progressing across the basin during the fall of 2002. Using the tracking approach described above, we identified 42 storms during the 4-month period. However, some of the storms merged and others split, so not all of the tracks were unique. Also, five of the storms were removed from the ensemble because they were too short-lived. The remaining storm tracks are shown in Fig. 4a. One sees that most of the storms entered the domain off Asia, south of 50°N, and progressed to the northeast while fanning out over a fairly wide range of latitude. This general pattern characterizes the main Aleutian low storm track. As mentioned in the introduction, there is a secondary path by which storms enter the Gulf of Alaska directly from the south. Figure 4b shows the five storms that followed such a route. In three of these cases the storms took a “sharp left” near 160°–170°W before going north, and in all cases the storms ultimately veered to the east. This pattern can be understood by considering the upper-level steering currents associated with these storms. Included in Fig. 4b is the average 500-mb height field for the five storms; the northeasterly oriented contours explain why none of the cyclones ended up in the central or western Bering Sea.

Our domain extended far enough north to capture five Arctic-born cyclones (distinct from Aleutian lows), whose tracks are shown in Fig. 4c. These storms remained in the Arctic domain, which is not surprising based on the zonally oriented upper-level steering currents. All of these storms occurred in late summer–early fall, which is the typical seasonal pattern for such storms that influence the southwestern Arctic (e.g., Wise et al., 1981; Zhang et al., 2004). We will not consider Arctic-born storms any further in this study.

The locations where each of the storms experienced their maximum deepening rate is shown in Fig. 5a (solid

¹ Note that there is some lateral extent to the notch; the arrow in Fig. 3c denotes the approximate centroid of the feature.

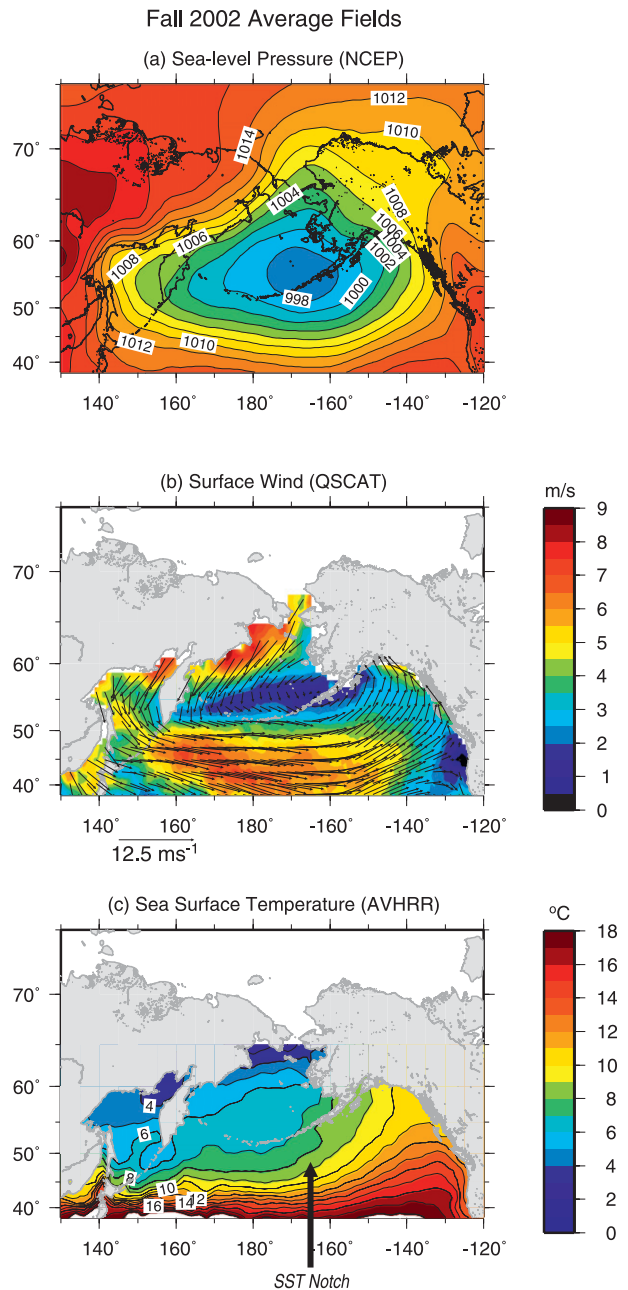


FIG. 3. Mean fields for fall 2002. (a) SLP (mb) from the NCEP data. (b) Surface vectors overlaid on wind speed (color), from QuikSCAT. The vectors were subsampled every sixth point. (c) SST from AVHRR. The SST Notch discussed in the text is marked by the arrow (which denotes the approximate centroid of the feature).

green circles), superimposed on the storm tracks. For comparison we also show the locations where the ensemble of polar lows studied by Businger (1987) deepened (solid stars, over the time period 1975–83). Polar lows are a different class of cyclone, with very short length scales (radius order 150–250 km) and short time

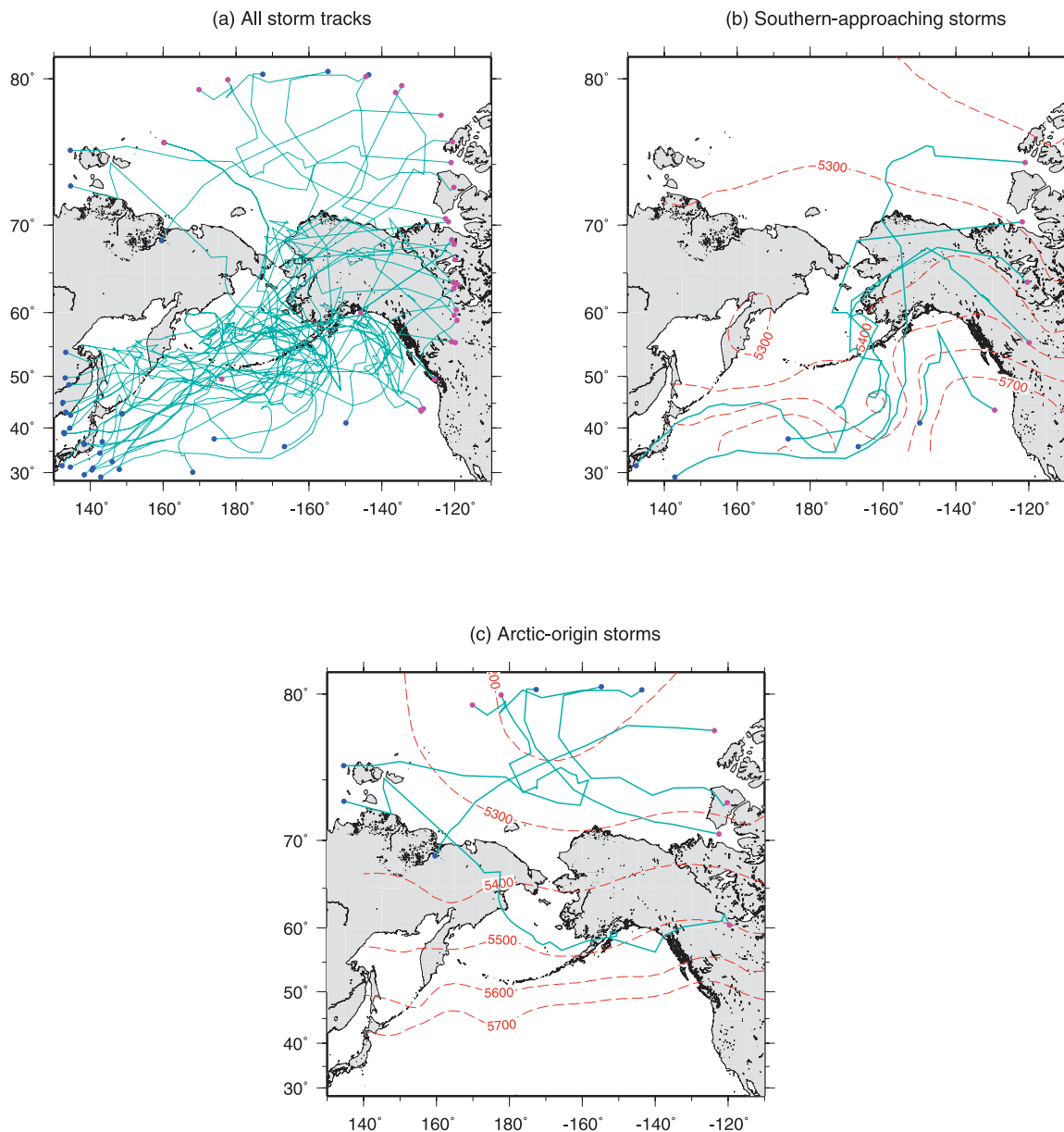


FIG. 4. Cyclone tracks (cyan lines) during fall 2002. The blue circles denote where the storms entered the domain, and the magenta circles show where they left the domain or spun down. (a) All storms. (b) Storms that entered the Gulf of Alaska from the south. The red dashed contours show the average 500-mb height field (m) during these storms. (c) Arctic-origin storms [red dashed contours defined as in (b)].

scales (less than a day). As discussed by Businger (1987), they form as a result of the contrast in surface temperature associated with the coastal landmass and the adjacent waters of the northern Gulf of Alaska (see Fig. 5a) and are not captured by the low-resolution NCEP fields. The general location where polar lows form is clearly distinct from that of the Aleutian lows.

As seen in Fig. 5a, in fall 2002 the Aleutian lows tended to deepen in two distinct geographical regions: in the Gulf of Alaska south of the Alaska Peninsula and farther to the

west in the region south of Kamchatka. As shown later, this pattern appears to be typical based on climatological data. It is also not surprising, based on past studies that have documented the enhanced storm activity in these two general areas (see the introduction). Below we investigate the reasons for this bimodal pattern. The median maximum deepening rate in our ensemble (adjusted for latitude) was $9.2 \text{ mb (12 h)}^{-1}$. To put this in perspective, a rate of $12 \text{ mb (12 h)}^{-1}$ is considered a “bomb” (Sanders and Gyakum 1980). By this criterion, roughly a third of the

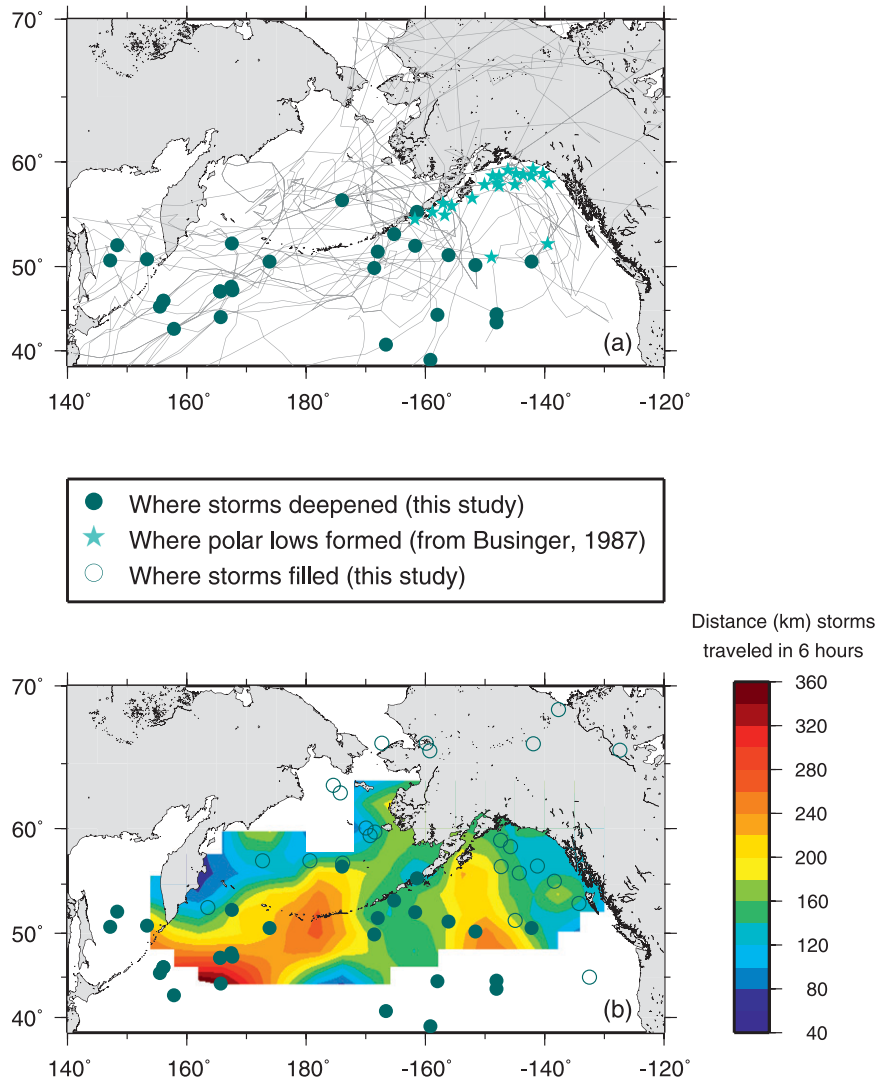


FIG. 5. (a) Locations where storms experienced their maximum deepening rate (solid green circles) compared to where polar lows deepened (cyan stars; from Businger 1987). Storm tracks are denoted by the gray lines. (b) Locations where storms filled (open green circles). The color denotes the distance the storms traveled (km) in a 6-h period.

storms in autumn 2002 experienced intense enough cyclogenesis to be considered bombs. The locations where the storms filled are indicated in Fig. 5b (open circles). Storms tended to spin down in the eastern Gulf of Alaska, as anticipated because of the nearby high coastal topography, and in the Bering Sea.

The geographical pattern of storm translation speed is intriguing in light of the observed patterns of cyclogenesis and spindown. As noted above, we calculated the distance traveled by the storms over each 6-h period, which is inherently noisy. To reduce this noise we gridded the domain into 2° latitude \times 4° longitude boxes, and computed the median distance traveled in each box that had at least five realizations. The resulting

distribution is shown in Fig. 5b (color), which shows some interesting patterns. As storms first enter the domain south of Kamchatka, they move swiftly and intensify. After continuing to the east at a fast rate, they tend to slow down near 160° – 170° W, which is the second area where intensification occurs. Note that the two areas where the translation speeds are most reduced—the eastern Gulf of Alaska and northwest Bering Sea—are where the storms tend to fill.

4. Seasonal storm evolution

We consider now the seasonal trends of storm development for our ensemble of low pressure systems.

Because it was our desire to focus on the typical behavior of Aleutian lows, we omitted the southern-origin storms from the analysis (which are much less common). In addition, we excluded storms that entered the domain in the far eastern part of the Gulf of Alaska (east of 140°W), storms that spun up in the Bering Sea, and storms that quickly merged with others. This reduced our ensemble to 22 storms. While it would have been desirable to have a larger sample size in terms of statistics, our approach was to perform an in-depth analysis of the storm evolution, including detailed consideration of each storm, which was only possible with a manageable number of realizations. The consistency of the results, and the subsequent climatological averages presented below, suggest that our conclusions are robust.

There was a clear seasonality to the development of the storms comprising the two clusters (east and west) in Fig. 5a. This is demonstrated by considering each of the clusters in turn.

a. Gulf of Alaska

Figure 6a shows the yearday of cyclogenesis of the low pressure systems in the eastern group of storms. As noted earlier, some storms experienced more than one period of deepening, and to increase the sample size of the eastern cluster we included all of the secondary deepening events as well (indicated by the stars in Fig. 6a, whose storms experienced their primary deepening near Kamchatka). There is a clear difference in that for the first part of fall, storms tended to spin up near 160°–170°W (the brighter colored symbols in Fig. 6a, south of the Alaska Peninsula), while in the latter part of the fall, storms deepened farther to the east in the central gulf (bluer symbols in Fig. 6a). We suspect that this is related to the seasonal development of the SST field.

Figure 7 shows the monthly mean SST field (color) for fall 2002. One sees the marked cooling that occurs in the Bering Sea and the progression of low temperatures into the Gulf of Alaska. A consequence of this is that the SST notch discussed above translates to the east as the fall progresses (from roughly 170°W in September to 145°–150°W in December). The imprint of this seasonally varying SST pattern on the lower troposphere is clearly seen in the monthly averaged 850-mb temperature field (Fig. 7, contours), which is typically ~1500 m above the sea surface and hence above the boundary layer. A similar bending of the isotherms occurs at 850 mb, and this feature translates to the east—in concert with the SST notch—as the season progresses. The translation in isotherms leads to a translation in baroclinicity in the lower troposphere, as illustrated by the 850-mb temperature gradient. The low-level baroclinicity shifts

from 160°–170°W in October to 145°–150°W in December (Fig. 7).

These areas of enhanced baroclinicity act as potential areas of cyclogenesis via baroclinic growth, given a suitable upper-level anomaly with which to interact. One can think of this growth in terms of coupled and interacting lower-level and upper-level potential vorticity (PV) anomalies (e.g., Hoskins et al. 1985). Figure 8 shows that the low-level baroclinicity induces a low-level PV anomaly, present throughout the lower troposphere, but illustrated here at the 600-mb level.² In October and November 2002 there is a well-defined PV anomaly at ~160°W, while in December 2002 this PV anomaly has translated to the east to ~145°W. These monthly mean PV anomalies follow the low-level temperature patterns. Transient upper-level PV anomalies would grow baroclinically (provided there was a westward tilt with height) by interacting with these low-level PV anomalies (Hoskins et al. 1985).

Such a configuration is illustrated in Fig. 9, which shows two different composite averages of the storms in Fig. 6a; the first for the storms that deepened before 15 November, and the second for those that deepened after 15 November. In each case, the composite consists of the 12-h time period encompassing the maximum deepening of the storms in question. The top of Fig. 9 shows the SLP field in relation to the SST, while the bottom shows the 500-mb height field in relation to the 850-mb air temperature. It is evident that in both time periods the storms deepened as they reached the SST notch (and the corresponding bend in the isotherms of the lower troposphere). On the bottom of Fig. 9 we have overlaid the PV isolines (thick contours) that define the PV max of Fig. 8. In particular, for the storms that deepened before 15 November (left-hand side) the location of the October PV max is shown, and for the storms that deepened after 15 November (right-hand side) the December PV max is shown. In both cases this represents a phase-locked cyclonic system, with a westward tilt with height—a configuration conducive to baroclinic growth.

The notion of the SST notch influencing storms may seem at odds with previous studies indicating that SST variability in the North Pacific is driven by atmospheric variability. However, this may be a matter of differing time scales. For example, Davis (1976) showed, using monthly averaged fields, that SLP anomalies lead

² PV is archived from the NCEP reanalyses on isentropic surfaces, and these diagnostics clearly demonstrate a vertically coherent PV anomaly in the lower troposphere. For illustrative purposes we have interpolated the PV onto a constant pressure level.

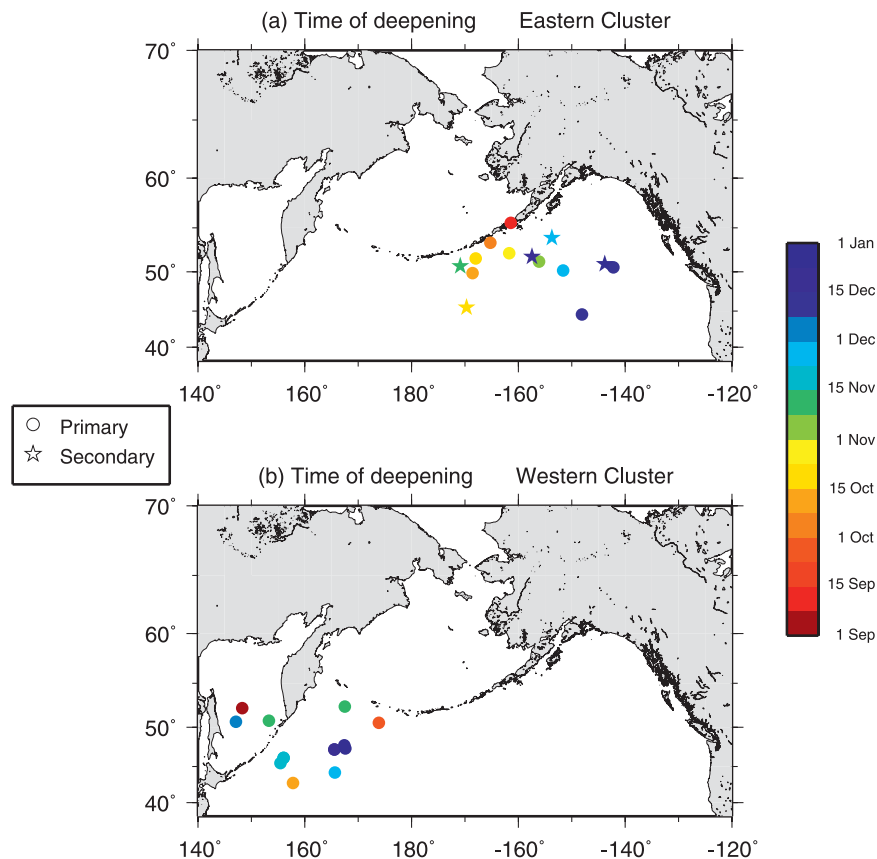


FIG. 6. Time of maximum deepening of the storms in Fig. 5a. (a) Storms in the eastern cluster. Included are storms that underwent a second deepening event in this region (denoted by the stars). (b) Storms in the western cluster.

those of SST. In contrast, we are asserting that there is a causal relationship between the synoptic behavior of storms and a quasi-permanent feature in the SST field. In particular, we argue that an individual storm reacts to the presence of the notch (or more specifically, the lower tropospheric potential vorticity structure that arises from the notch). The SST notch in turn responds to the cumulative effect of repeated storms that bring cold air from the north, which causes the notch to slowly progress to the east. Hence, we believe our results do not contradict the earlier North Pacific studies. In a broader context, Kushnir et al. (2002) review the atmospheric response to extratropical SST anomalies from general circulation model experiments. They discuss how the low-level temperature field in the atmosphere can indeed be influenced by the SST field but that this is just one factor in explaining the location and variability of storm tracks. We believe that for the Aleutian low at this time of year, the SST notch is influential in determining areas of low-level baroclinicity and thus enhanced cyclogenesis.

b. Western North Pacific

The timing of rapid deepening of the western cluster of storms also offers some clues as to the nature of the spinup process. Note in Fig. 6b that 9 of the 12 storms in this group deepened after 9 November. Also, the six strongest deepening events occurred after the middle of November. This implies that the main factors leading to the cyclogenesis in this region were more effective in the late fall. To shed light on this, we considered two groups of storms. The first group consists of five storms that passed through this region before 31 October and did not deepen substantially; they experienced their maximum deepening farther downstream as part of the eastern cluster of storms (Fig. 6, top). The second group contains four storms in the western cluster that deepened close to each other south of Kamchatka after 20 November. Figures 10a,b show the composite averages of SLP and SST for these two groups of storms, plotted the same way as in Fig. 9. In both instances the composite storm is located in approximately the same location, but in the early fall composite the storm is weaker.

Monthly-average SST (color) and 850 mb air temperature (contours) for fall 2002

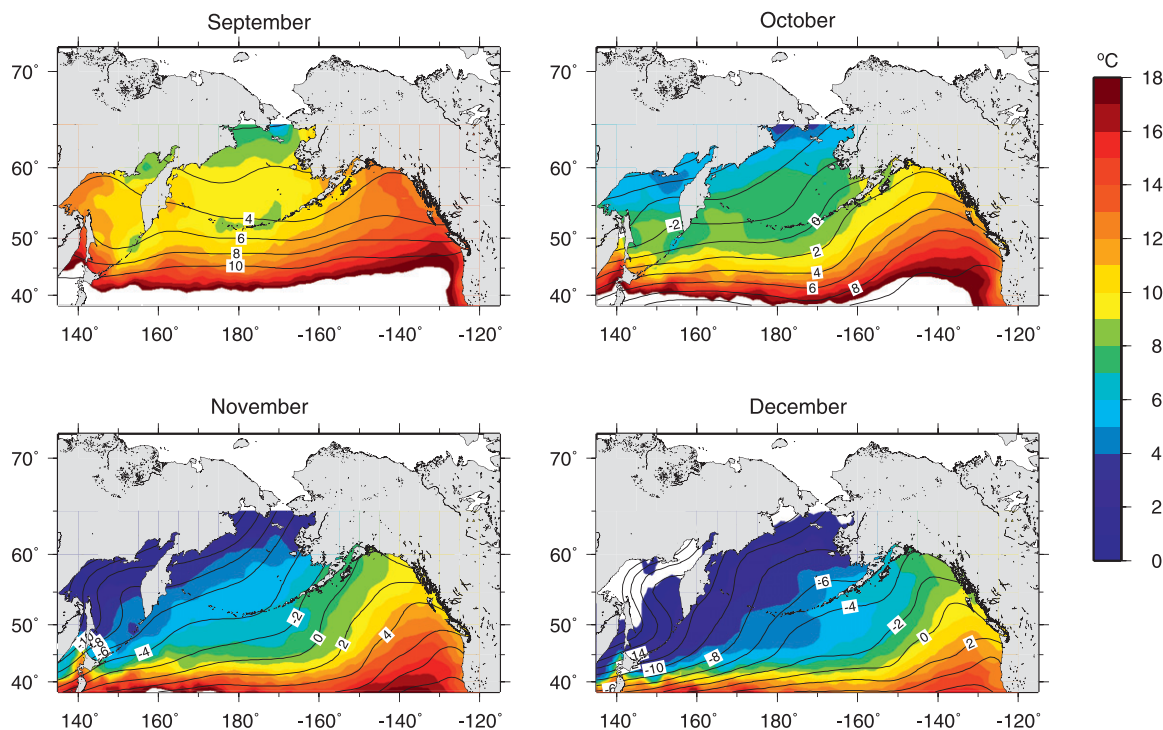


FIG. 7. Monthly averaged SST (color) from AVHRR and 850-mb air temperature (contours) from NCEP for fall 2002.

The other noticeable difference is that the SST is higher (not surprisingly) in early fall, north of the storm axis.

Why did the storms deepen later in the fall but not earlier? There are several possibilities. Close inspection of Figs. 10a,b suggests that one factor might be the latitude of the storm tracks, because four of the five storms that did not deepen were located farther north than the storms in the other composite that did. To investigate this, statistics for all of the storms were tabulated (over all months) as they passed Kamchatka. None of the cyclones deepened when located north of 50°N (seven total), suggesting that the latitude of the storm does play a role, perhaps because the storm is too far removed from the warm air south of the SST front. However, there is no significant seasonal trend in the latitude of the storm tracks in our ensemble, suggesting that storm position is not a factor in the difference between the two composites of Figs. 10a,b. Another possibility is the magnitude of the SST gradient, because at first glance it seems as if the gradient is stronger in the late fall composite. However, we quantified the gradient in the two composites near Kamchatka, and they are in fact comparable.

We believe that an important factor promoting storm development late in the season is the extreme cold, dry air that streams off the Asian landmass as winter approaches. To elucidate this, time series of surface air

temperature and specific humidity were computed in the boxed region in Fig. 10 north of the Sea of Okhotsk. Both the temperature and humidity decrease significantly through September and October, and (aside from some mild spells in early November) they remain low for the rest of the fall (Fig. 10c). However, for the cold, dry air to maximize the baroclinicity of the atmosphere it must remain largely unmodified as it passes southward over the Sea of Okhotsk. This would strengthen the contrast between the continental-origin air and the subtropical maritime air of the North Pacific that fuels these storms. To investigate this, two individual storms were considered. The first storm occurred in early October and did not deepen significantly, and the second occurred in late November and experienced intense cyclogenesis (Figs. 11a,b). Part of the reason these two particular storms were chosen is that the magnitude of the winds over the Sea of Okhotsk was nearly identical in each storm.

To quantify the modification of air passing over the Sea of Okhotsk, we computed the distribution of various properties along the two white lines shown in Figs. 11a,b, which are assumed to be approximate trajectories. This assumption is reasonable because the translation speed of the storms was such that they didn't move very much during the time it took an air parcel to

Monthly-averaged PV (color) and wind vectors at 600 mb for fall 2002

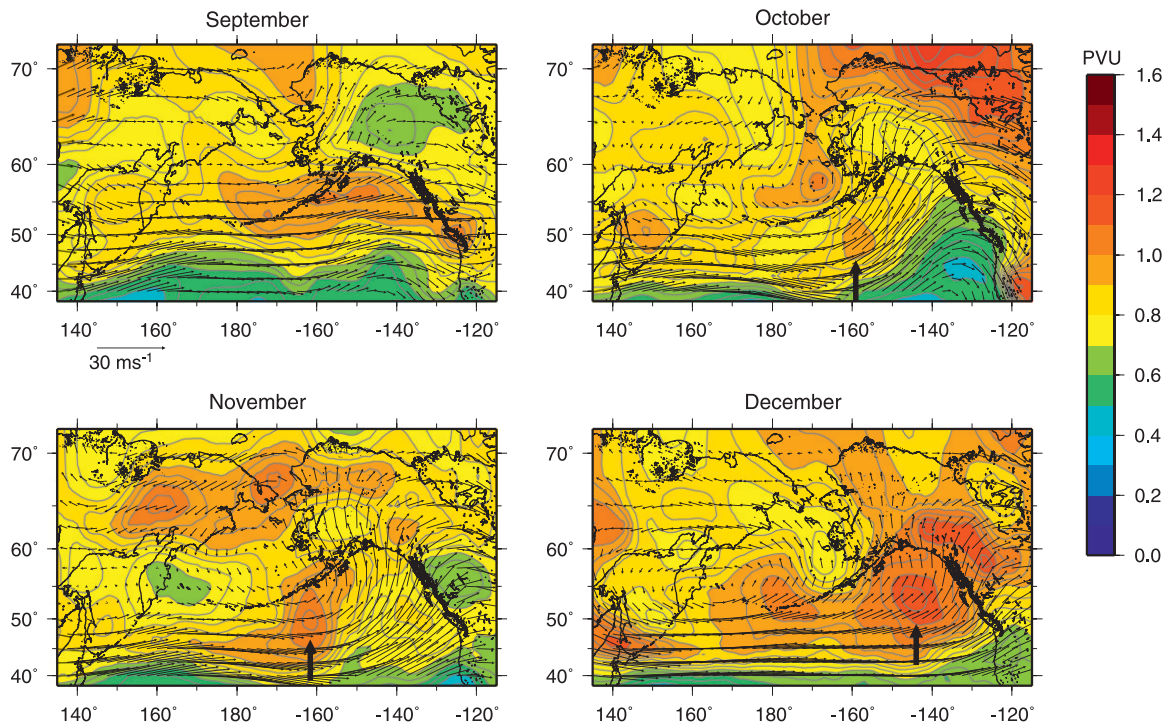


FIG. 8. Monthly averaged potential vorticity at 600 mb (color, $10^{-6} \text{ m}^2 \text{ s}^{-1} \text{ K kg}^{-1}$) overlaid by the wind vectors, from NCEP for fall 2002. The region of enhanced cyclonic vorticity discussed in the text is indicated by the arrow.

traverse the length of the lines. The surface air temperature and specific humidity distributions are plotted in relation to the SST in Figs. 11c,d. In the early storm, the air passing over the Sea of Okhotsk warms and moistens considerably. By contrast, the cold SST in the Sea of Okhotsk in late fall keeps the air chilled and significantly drier than in the earlier storm. This suggests that low pressure disturbances passing by this area will experience a greater contrast of air masses late in the season, and the resulting enhanced baroclinicity could be the cause of the greater number of strengthening events in late fall–early winter. Consistent with this notion is the fact that the 850-mb air temperature gradient across the later storm in Fig. 11 was stronger by a factor of 2 than that across the earlier storm.

c. Climatological progression

To summarize, the seasonal progression of storm evolution during autumn 2002 occurred as follows: in early fall, cyclones generally followed the North Pacific SST front to the east but did not intensify until they reached the vicinity of the SST notch, near the middle of the Aleutian Island chain. We have made the case that the imprint of the notch on the lower tropospheric air temperature, and the resulting enhancement of cyclonic

potential vorticity, likely influenced the cyclogenesis in this area. As fall progressed, the SST notch moved farther to the east, and correspondingly the location of cyclogenesis shifted eastward into the Gulf of Alaska. Shortly thereafter (with some overlap) storms started to deepen much farther to the west as they first entered the domain near Kamchatka. We surmise that at some point late in the fall the combination of cold, dry air leaving the continent, and the reduced modification of the air over the Sea of Okhotsk, resulted in enhanced atmospheric baroclinicity and thus cyclogenesis. The overall result is that there were two distinct areas of storm development in the North Pacific, which occurred slightly out of phase as the fall progressed.

Is the seasonal evolution observed in fall 2002 representative of a typical fall? To answer this we computed the climatological monthly averaged fall progression of SLP using the NCEP data over the nearly 60-yr period from 1948 to 2006 (Fig. 12). One sees that in September there is a weak signature of the Aleutian low near the Alaska Peninsula, which propagates to the east and intensifies in the October average. Note, however, that in November the signal stretches far to the west with a hint of increased intensity there. Then in December the low becomes deepest in the western region.

Composite averages of deepening events

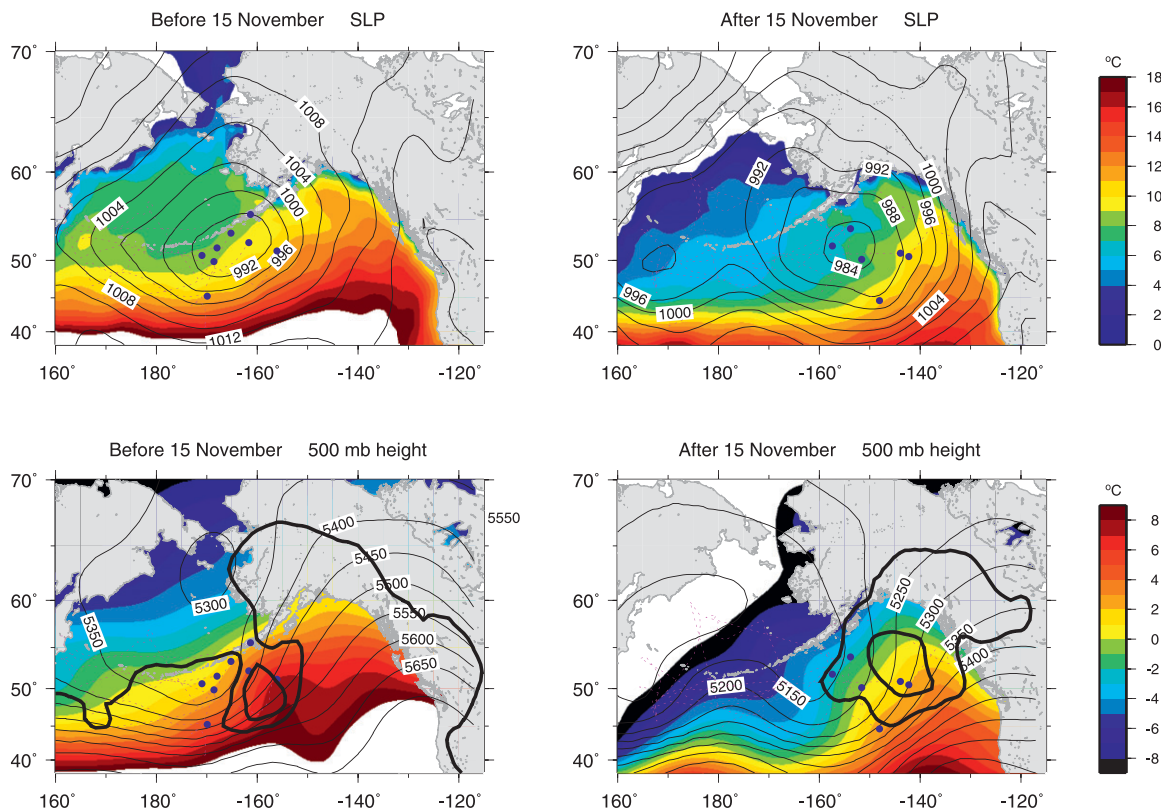


FIG. 9. Composite averages of deepening events for the eastern cluster of storms in Fig. 6. (left) Those storms that deepened before 15 November, and (right) those that deepened after 15 November. For each storm in the composite, the 12-h period bracketing the maximum deepening is included. (top) Mean SLP (contours, mb) overlaid on the mean SST (color). (bottom) The mean 500-mb height field (thin contours, m) overlaid on the mean 850-mb air temperature (color). Also shown on the bottom row are selected PV isolines (heavy contours) defining the PV max of Fig. 8 in October [(left) PV = 0.85 and 0.9] and December [(right) PV = 1.0 and 1.1]. The locations of the storms at the time of maximum deepening are denoted in all plots by the blue circles, and the trajectory of the storms preceding this are indicated by the magenta dashed lines.

This progression is similar to that presented in Favorite et al. (1976) based on 20 yr of shipboard observations. It is also exactly as one would expect based on the seasonal pattern of cyclogenesis described above for fall 2002; indeed the monthly SLP progression for fall 2002 follows this same pattern. To verify that the NCEP climatological pattern is reflective of storm development (and not an artifact of averaging), we identified the location of minimum SLP for each of the individual months of October and December. These locations are indicated by the crosses in Fig. 12. One sees that on a monthly basis, the Aleutian low signature was located primarily in the Gulf of Alaska in early fall, versus the western Pacific in late fall. There is more scatter in December, but even during those months when the minimum SLP was not in the western Pacific, there was usually a weaker isolated low located there. This implies that the results presented above for 2002 are represen-

tative of the canonical storm development in the North Pacific during autumn.

5. Implications for the North Pacific subarctic gyres

The fact that there are two distinct regions of enhanced cyclogenesis in the North Pacific, each of which will be associated with a different pattern of wind stress curl, is likely to impact the subpolar ocean circulation. To address this we considered the historical database of hydrographic stations in the North Pacific Ocean to make some inferences regarding the surface circulation.

a. Overview of the circulation

The general circulation of the North Pacific is shown schematically in Fig. 13. The North Pacific Current (fed by the Kuroshio Extension) flows eastward and, upon reaching the eastern boundary, splits to form the

Composite averages of events

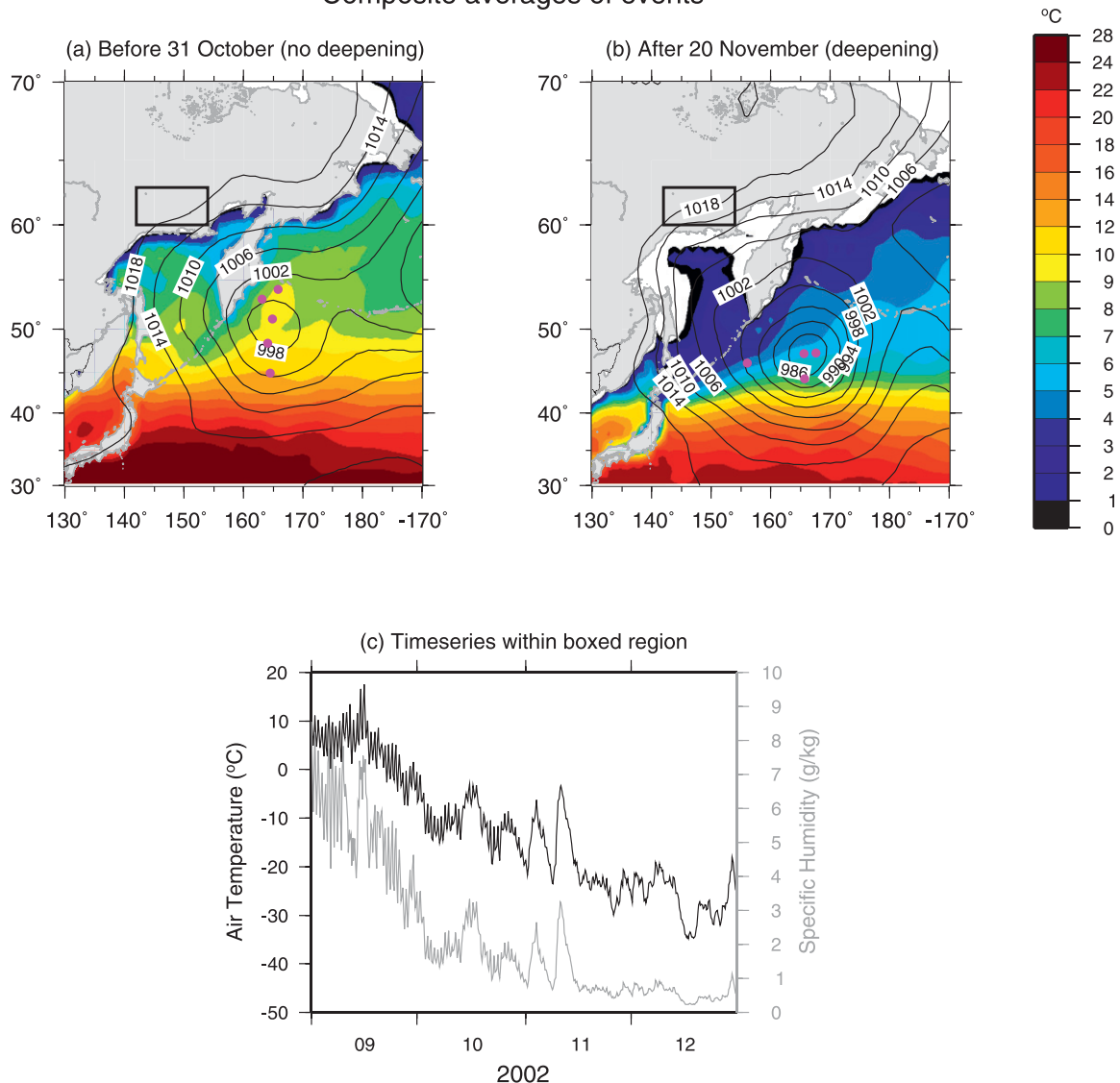


FIG. 10. Composite averages of SLP (contours, mb) overlaid on SST (color) for (a) storms near Kamchatka before 31 Oct that did not deepen and (b) storms after 20 Nov that did deepen. For each storm in the composite, the 12-h period bracketing the maximum deepening is included. (c) Time series of surface air temperature (black line) and specific humidity (gray line) within the boxed region in (a), (b).

northward-flowing Alaska Current and southward-flowing California Current. The northward flow then bends to the west and becomes the Alaskan Stream, which flows along the Alaska Peninsula and Aleutian Island arc. This is the western boundary current of the cyclonic Alaska gyre. Some portion of the Alaskan Stream flows northward through the passages in the Aleutian Island chain and enters the Bering Sea (e.g., Stabeno et al. 2005), participating in the cyclonic circulation of that basin (e.g., Cokelet et al. 1996). Some authors refer to this as the Bering Sea gyre (e.g., Favorite

et al. 1976), while others consider this as part of the larger western subarctic gyre. In Fig. 13 the latter terminology has been used. The western boundary current of the western subarctic gyre is known as the Kamchatka Current in the north and the Oyashio Current in the south. Some studies consider the circulation in the North Pacific as a single large-scale subarctic gyre with intensification in the east and west. However, there is enough evidence—for instance, from surface dynamic topography (see Favorite et al. 1976; Qiu 2002; and the analysis below)—to suggest that two distinct gyres do

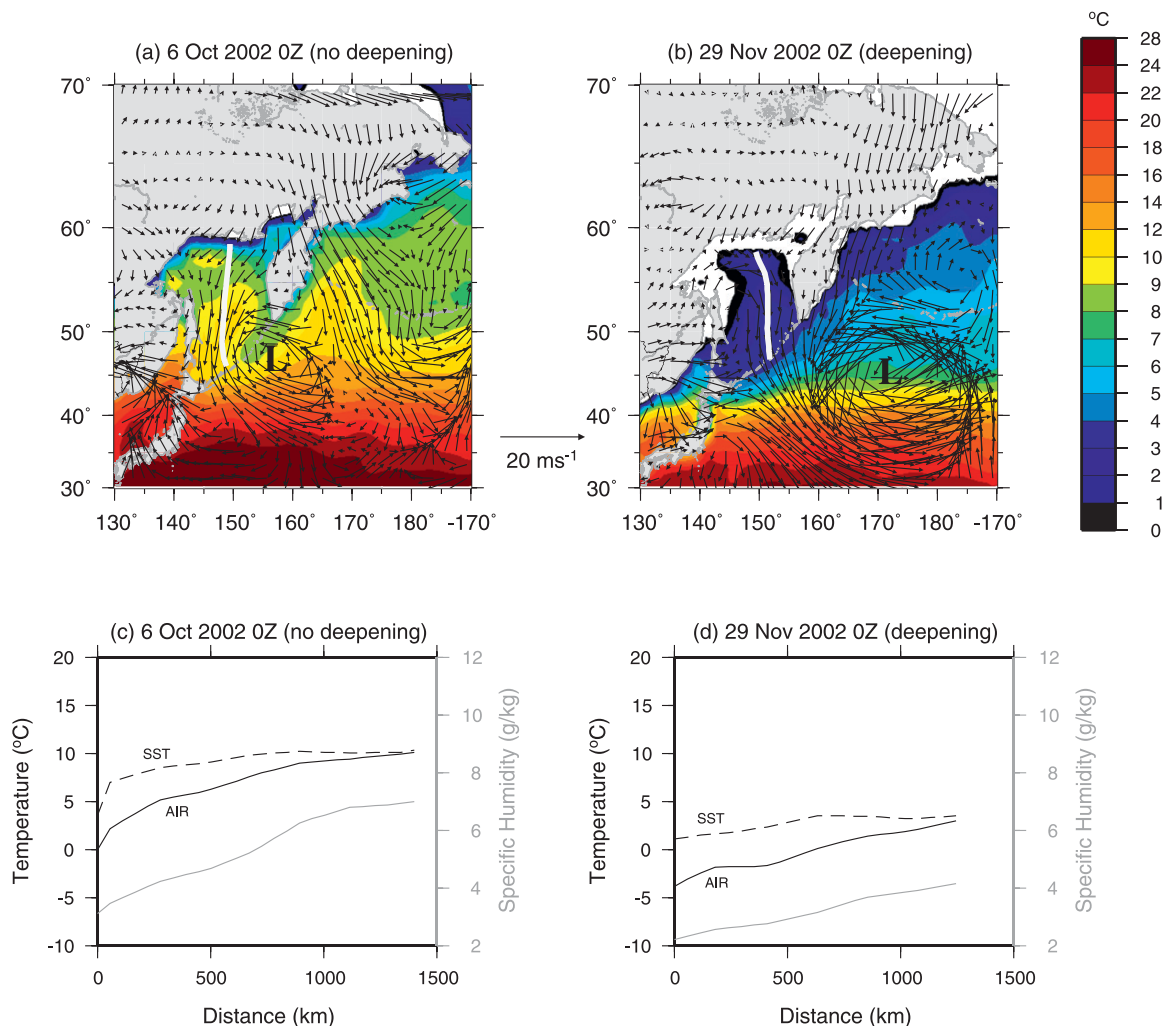


FIG. 11. Comparison of two storms south of Kamchatka. (left) The storm in early October did not deepen. (right) The storm in late November experienced intense cyclogenesis. (top) The 10-m wind vectors overlaid on SST (color). The storm center is depicted by the large L. The white lines are the approximate trajectories discussed in the text. (bottom) The evolution of properties progressing southward along the white lines.

indeed exist as depicted in Fig. 13. The precise transition between the two gyres remains unclear, however.

The strength of the Alaska gyre has been estimated by measuring the strength of the Alaskan Stream (e.g., Reed et al. 1980; Royer 1981; Musgrave et al. 1992). Summaries of the transport estimates of this flow have been given by different authors (see the discussion in Cokelet et al. 1996). Essentially, geostrophic calculations referenced to 1000–1500 db give transports in the range of 5–16 Sv (1 Sv $\equiv 10^6 \text{ m}^3 \text{ s}^{-1}$; Cokelet et al. 1996). However, it is believed that these are underestimates due to the presence of significant thermal wind shear at deeper depths and due to the barotropic component of the flow. Musgrave et al. (1992) estimate that the baroclinic transport values computed in their study, referenced to 1000 db, are too

small by a factor of 2. Geostrophy referenced to current meter records and to shipboard acoustic Doppler current profiler data boosts the transport of the Alaskan Stream to 23–24 Sv over the upper 1500 m (Warren and Owens 1988; Cokelet et al. 1996) and to 28 Sv for the entire water column (Warren and Owens, 1988).

Similar uncertainty exists for the western subarctic gyre. Its strength can be estimated by considering the transport of the Kamchatka and Oyashio Currents. Baroclinic estimates of these flows range from 5 to 23 Sv for the Kamchatka Current (Cokelet et al. 1996, and references therein), and 9 to 14 Sv for the Oyashio Current (Uehara et al. 2004, and references therein). More recent estimates of the absolute flow suggest that the high end of this range is perhaps more accurate. For example,

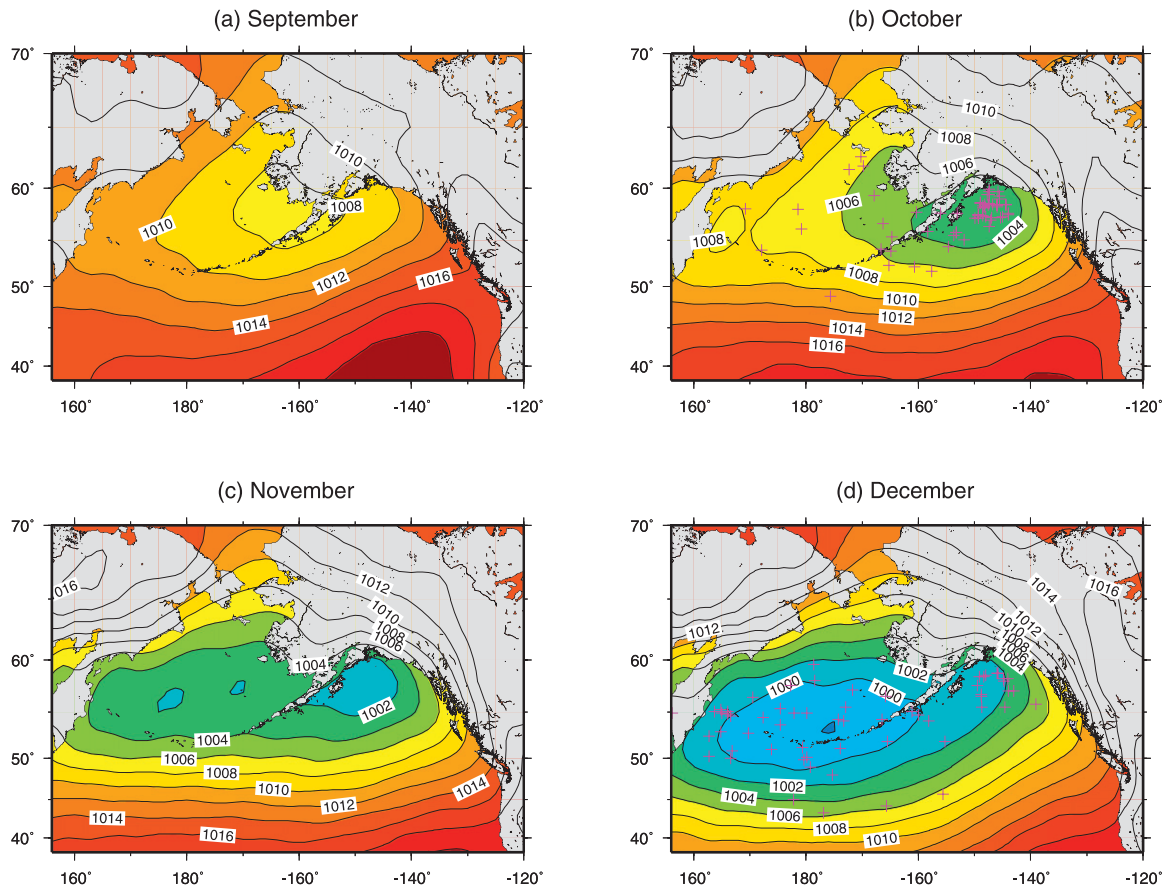


FIG. 12. NCEP Climatological mean SLP for (a) September, (b) October, (c) November, and (d) December, during the period 1948–2006. For October and December, the magenta pluses denote the location of the minimum SLP for the individual months comprising the climatology.

Pantelev et al. (2006) performed an inverse calculation using various sources of oceanographic and atmospheric data and deduced a transport of 24 Sv for the Kamchatka Current. Uehara et al. (2004) showed that relative transport estimates of the Oyashio Current were increased substantially when referenced using mooring data. They reported a month-long full-water-column transport in winter 2001 of 31 Sv. Hence, for both the Alaska gyre and the western subarctic gyre, the absolute transports appear to be over 20 Sv, although Uehara et al. (2004) mention that in general, the transport of the western gyre seems to be less than the eastern gyre.

Why are there two subarctic gyres? There seem to be two prevailing notions, both of which are related to the geography of the region. The first idea is that the northward flow through the Aleutian Island chain helps to establish the western gyre. Using current meter arrays, Stabeno et al. (2005) report that >4.5 Sv flow northward through four of the passages into the Bering Sea. This flow initially forms the eastward-flowing Aleutian North Slope Current (Stabeno et al. 1999), which even-

tually feeds the cyclonic circulation of the Bering Sea. This pattern is shown clearly in the numerical model of Overland et al. (1994). The flow eventually returns southward in the Kamchatka/Oyashio Currents.

The second idea pertains to the orientation of the Aleutian Island arc. As investigated by Thomson (1972), when the Alaskan Stream flows southwestward the change in planetary vorticity can be balanced by lateral diffusion of vorticity due to the presence of the boundary, as usual for a western boundary current. However, this dynamical balance cannot hold west of where the island arc bends to the north (west of 180°W) because the planetary vorticity of the flow increases, yet the sign of lateral vorticity diffusion remains the same. This in turn would imply a separation of the flow from the boundary. The model of Overland et al. (1994) shows flow separation in this region: in the mean, the separated Alaskan Stream continues zonally to the western boundary where it joins the Kamchatka Current. This pathway is consistent with drifter observations (Stabeno and Reed 1992), and water of Alaskan

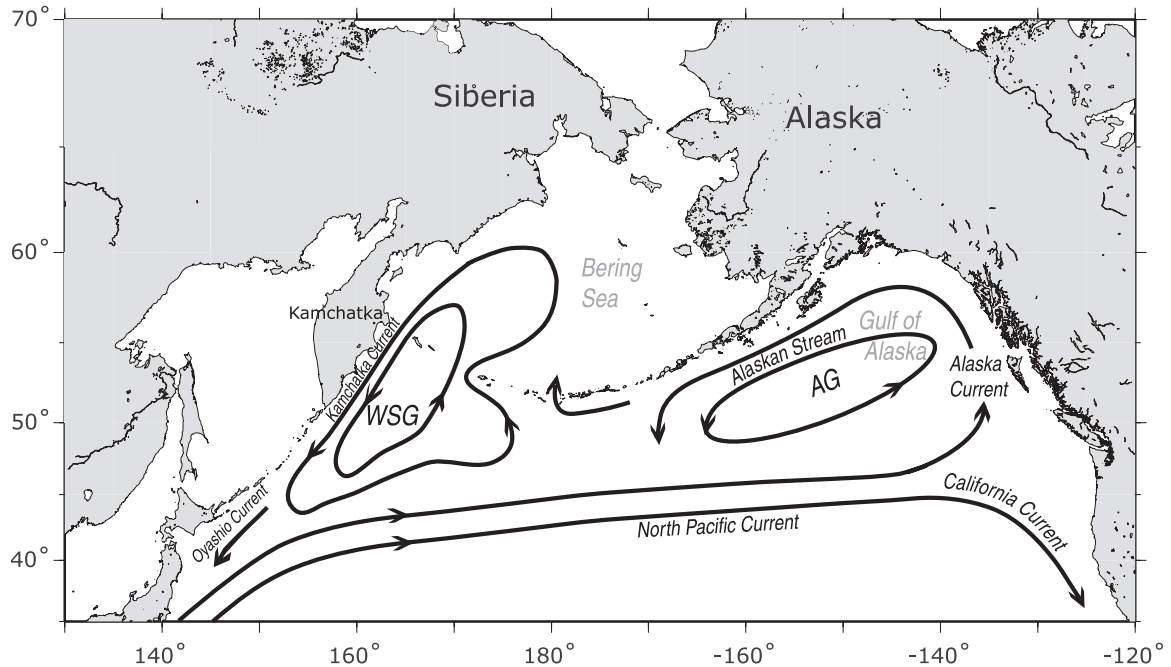


FIG. 13. Schematic of the upper-layer circulation of the North Pacific Ocean. AG stands for Alaska gyre and WSG stands for western subarctic gyre.

Stream origin makes it far to the west at this latitude (Favorite et al. 1976). However, near the separation point, at the apex of the Aleutian Island chain, Overland et al.'s (1994) model shows large-amplitude meanders of the current, suggesting instability. This is consistent with observations of eddy formation in this region (Cokelet et al. 1996) and with distributions of salinity showing Alaskan Stream water entering the interior (see Thomson 1972). The idea then is that some of the separated flow recirculates, forming the western limb of the Alaska gyre. Note that the discrepancy in transport discussed by Uehara et al. (2004) between the Alaskan Stream and the Kamchatka/Oyashio Currents is consistent with the notion of recirculation.

We argue below that the distribution of vorticity input from the wind, due to the bimodal storm pattern, may also be part of the reason why there are two distinct subpolar gyres in the North Pacific.

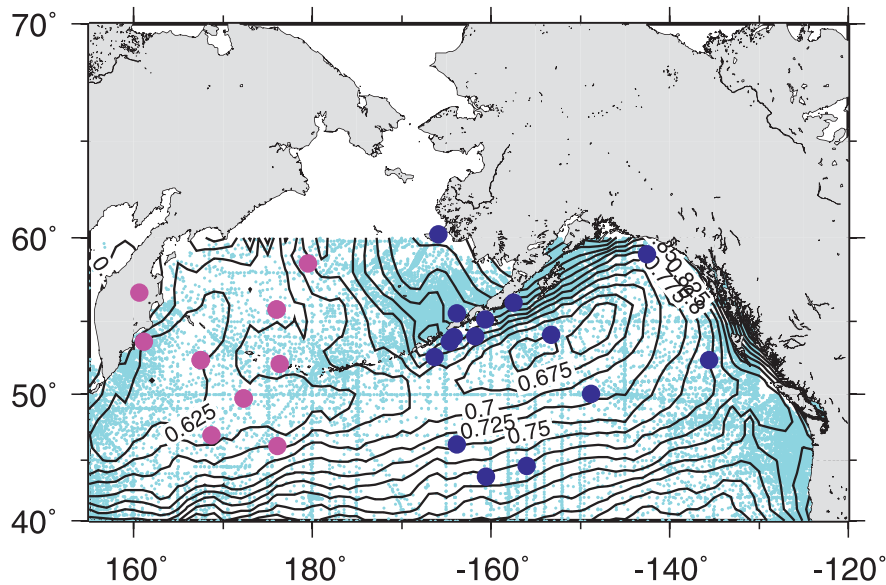
b. Wind stress curl and surface flow

The mean surface dynamic topography of the North Pacific, based on more than 60 yr of data, is shown in Fig. 14 (contours). For this calculation we used a reference pressure of 500 db, but the pattern is insensitive to this choice (e.g., a level of 250 or 1000 db gives essentially the same distribution). The two subpolar gyres are clearly evident; note that the western gyre extends into the Bering Sea. This pattern is similar to that presented in Favorite et al. (1976, their Fig. 26), who used

station data from the National Oceanographic Data Center prior to 1973. The pattern is also similar to Qiu's (2002) mean surface dynamic topography distribution constructed using the Levitus climatology. The locations where the ensemble of storms during fall 2002 reached their minimum pressure are overlaid on the dynamic topography of Fig. 14a. Interestingly, the two clusters of storms are centered near the two gyres. To elucidate this we computed the composite wind stress curl distribution associated with these minimum pressure time periods, which is shown in Fig. 14b (color). This reveals that there are two distinct regions of enhanced cyclonic wind stress curl that are located near the two cyclonic ocean gyres.

The wind stress curl composite of Fig. 14b is of course based on data from autumn 2002 only—we show this because it demonstrates that a bimodal curl signature results from the storms spinning up in two separate geographical regions as examined above. Does such a bimodal curl pattern exist in the climatology? Figure 15 shows the climatological wind stress curl, where the year has been divided into two time periods: from October to March (roughly the storm season) and April to September. The top panel, which uses the 60-yr NCEP average, shows two regions of strong cyclonic curl on the two sides of the basin, which largely disappear in the spring and summer months. Keep in mind that NCEP data were used to conduct the storm analysis presented above. The magnitude of the curl in winter is strong

(a) Surface dynamic topography and locations where storms reach minimum pressure



(b) Surface dynamic topography with curl overlaid

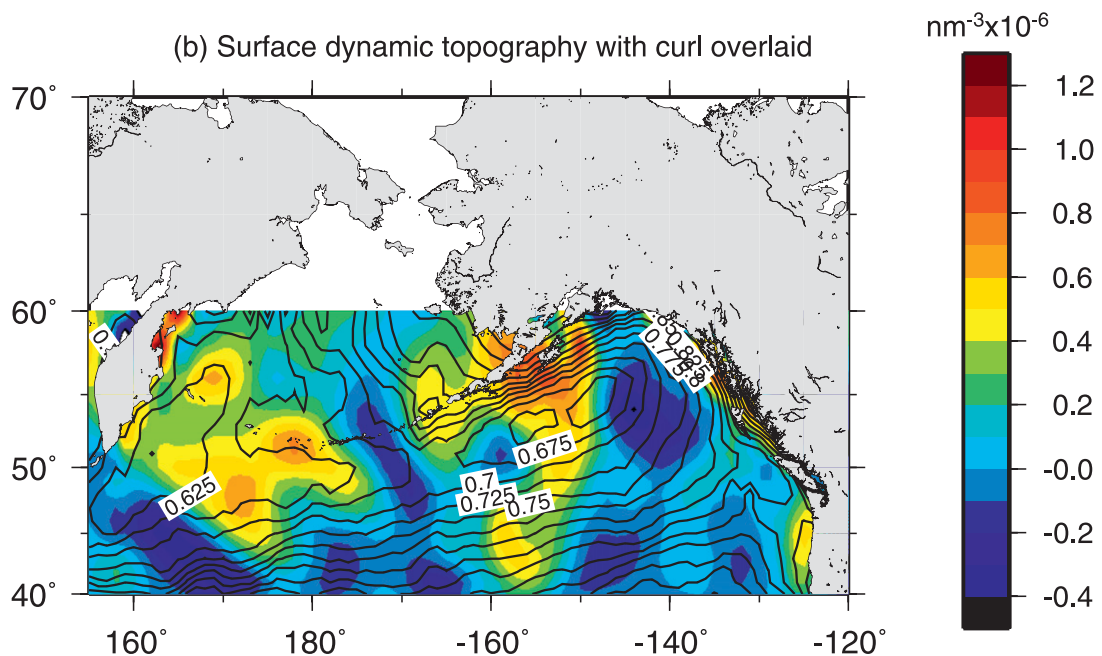


FIG. 14. (a) Mean surface dynamic topography (contours, referenced to 500 dbar) over the period 1940–2000, from the HydroBase 2 climatology. Hydrographic station locations are marked by the cyan dots. The circles denote where the storms in autumn 2002 (Fig. 5a) reached their minimum pressure. The magenta circles correspond to the western cluster of storms, and the blue circles correspond to the eastern cluster of storms. (b) The dynamic topography in relation to the composite average wind stress curl (color) from both clusters of storms in (a).

enough that this bimodal pattern is present in the 12-month climatological average as well (with a weaker amplitude). For comparison we computed the analogous half-year composites of wind stress curl using the QuikSCAT

surface wind data, which covers only the period since 1999 (Fig. 15, bottom). One sees that the general patterns are similar, that is, enhanced curl in the west and east, which is present only during the storm season (but

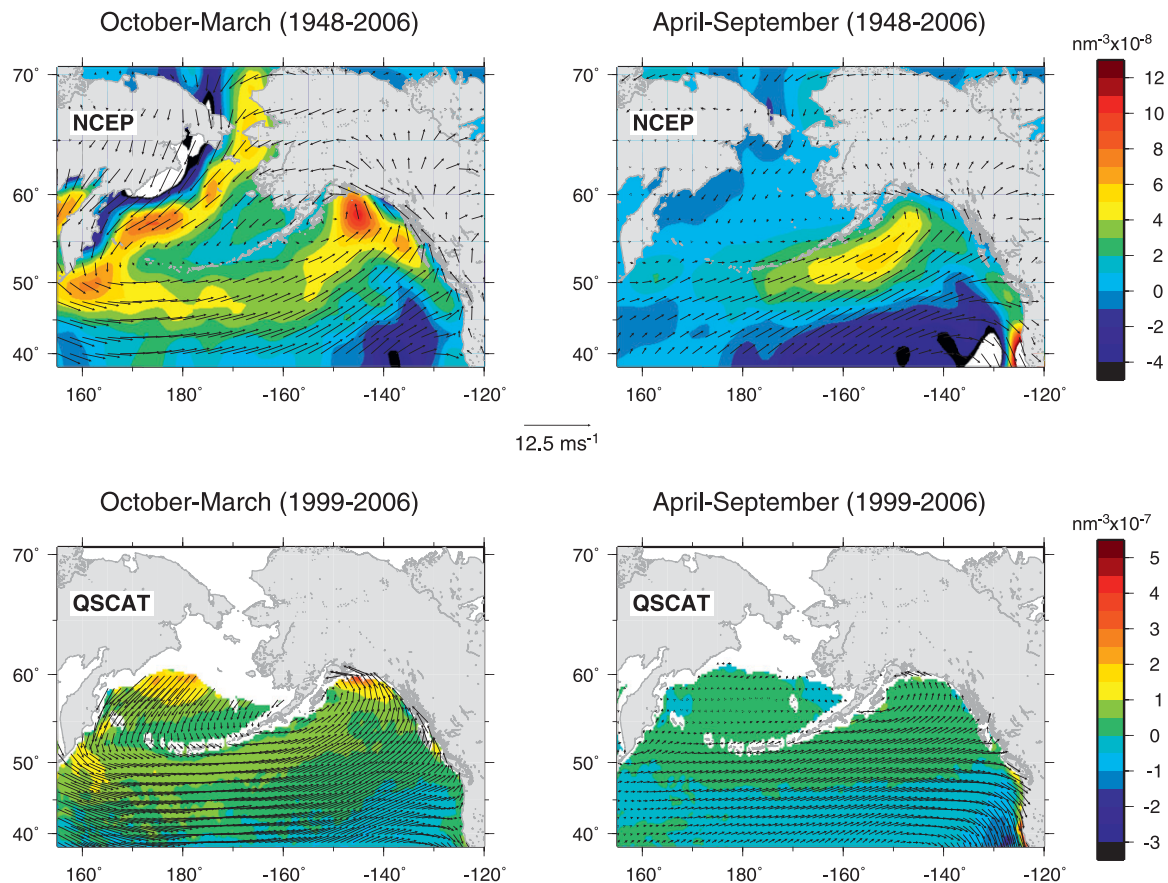


FIG. 15. Climatological wind stress curl (color) and wind vectors for the two 6-month periods (left) October–March and (right) April–September. The top row uses NCEP data for the period 1948–2006 (10-m winds), and the bottom row uses QuikSCAT data for the period 1999–2006 (surface winds, subsampled every fifth point). Note the different color scale used for the QuikSCAT-derived curl.

strong enough to show up in the annual average). Finally, we note that the mean curl distribution computed from 10 years of ERS wind data (1991–2000) shows a similar pattern (discussed below), as does Kutsuwada’s (1982) wind stress curl distribution calculated using ship reports from 1961–75.

6. Discussion

It is clear from the above analysis that one of the robust features of the wind field over the North Pacific is the presence of two enhanced areas of cyclonic wind stress curl, and that these are geographically associated with the two subpolar gyres. The curl pattern arises because of the tendency of cyclones to deepen in two distinct regions over the course of the storm season. While we suspect that the collocation of the cyclonic wind stress curl signal and the two ocean gyres is not a coincidence, it still needs to be demonstrated how such a seasonal input of vorticity can drive a mean double-gyre circulation. While a rig-

orous investigation of this hypothesis is beyond the scope of our study, we are able to offer a few insights.

A similar bimodal seasonal input of cyclonic vorticity occurs in the subpolar North Atlantic, associated with the passage of storms along the North Atlantic storm track (see Fig. 2 of Spall and Pickart 2003). Two regions of enhanced cyclonic wind stress curl develop every winter, one on each side of southern Greenland. Furthermore, there are two local cyclonic recirculation gyres that are part of the year-round circulation of the western North Atlantic: one to the east of Greenland in the Irminger Sea, and one to west of Greenland in the northern Labrador Sea (see Lavender et al. 2000). Spall and Pickart (2003) modeled this scenario and demonstrated that even with seasonal wind forcing, a permanent circulation exists similar to that observed by Lavender et al. (2000). Spall and Pickart (2003) also showed that the seasonal signal of the gyres should be small compared to the amplitude of the mean circulation, as is observed (Lavender 2001). One of the reasons for this

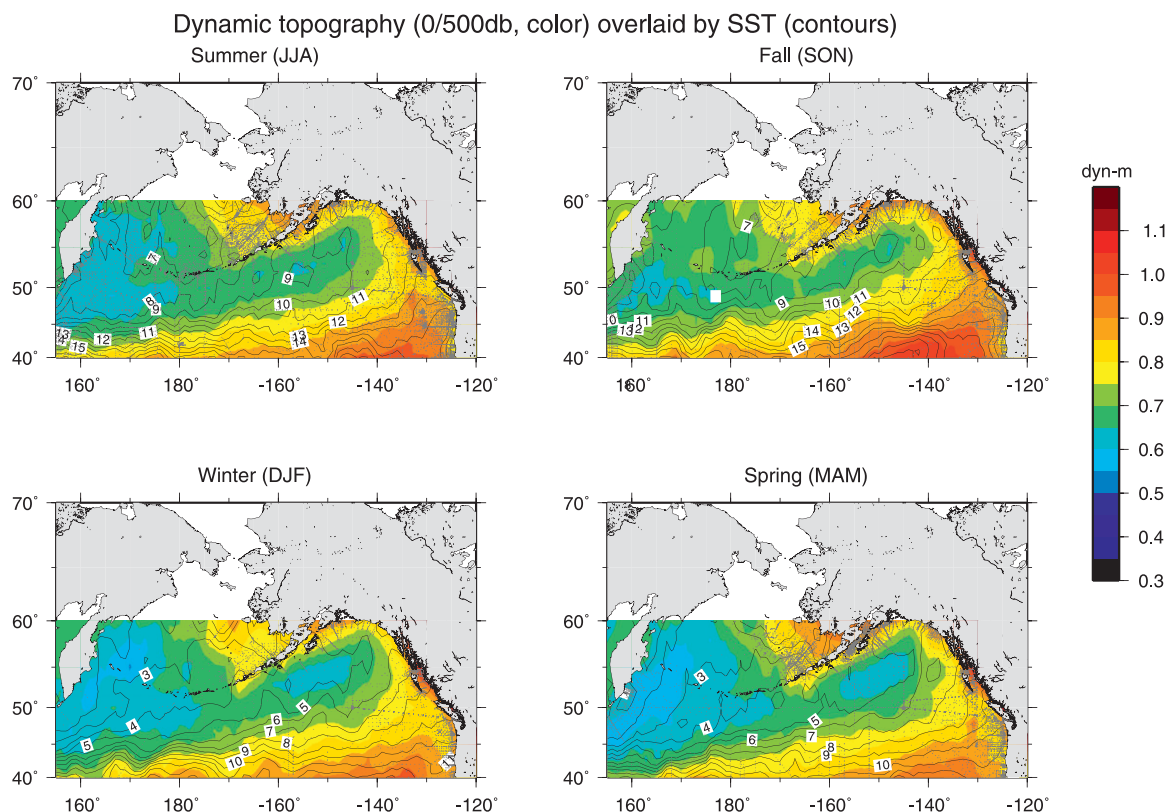


FIG. 16. Climatological seasonal surface dynamic topography referenced to 500 dbar (color), overlain by SST ($^{\circ}\text{C}$, contours). Summer (June–August); fall (September–November); winter (December–February); spring (March–May). Station locations are marked by the gray dots.

is that the baroclinic Rossby wave response to the wind forcing is very slow, and hence the circulation is unable to adjust fully (i.e., spinup to the level that the gyre would attain if the wind forcing were steady). A second important element is the bottom topography and its impact on the deep flow, which tends to counteract the upper ocean response and therefore damp the seasonal variation.

The seasonality of the two North Pacific gyres is not very well established, although some aspects have been identified. For instance, it is clear that seasonal variations of the Alaska gyre are small. Favorite et al. (1976), Reed et al. (1980), and Musgrave et al. (1992) detected no significant annual signal in the Alaskan Stream. Royer (1981) computed a seasonal transport amplitude (referenced to 1500 db) of 1.2 Sv, with a maximum in March (versus a mean of 9.2 Sv). Using Ocean Topography Experiment (TOPEX)/Poseidon altimeter data, along with assumptions about scales, Qiu (2002) deduced an annual variation in the Alaska gyre of ± 1.4 Sv, with the maximum intensity occurring in January–March. For the western subarctic gyre there also seems to be some intensification in winter. For instance, Uehara et al. (1997) and Uehara et al. (2004) noted stronger wintertime flow

of the Oyashio Current, although they were unable to quantify the seasonal amplitude. Qiu's (2002) annual signal for the western subarctic gyre from altimetry was ± 4 Sv, while Overland et al.'s (1994) model produced a seasonal amplitude of ± 2.5 Sv (both with the maximum signal in winter). In light of the recent larger estimates of mean gyre transports noted above (> 20 Sv), the conclusion seems to be that the two North Pacific gyres tend to strengthen in winter, but that the seasonal amplitude is significantly less than the mean.³ This is also the case according to our analysis of the historical hydrography. While there are much less station data in the winter months, a clear pattern emerges showing that both gyres intensify somewhat during winter and spring (Fig. 16).

It is evident that the situation in the North Pacific has notable similarities to the North Atlantic case. Both basins have two regions of cyclonic wind stress curl on either side of a curved boundary (in the Pacific the

³ The strong variability in Oyashio transport over the period 1992–94 reported by Kono and Kawasaki (1997) seems to be an exception to this, but they had only 2–3 realizations per year, which is not enough to quantify the annual signal.

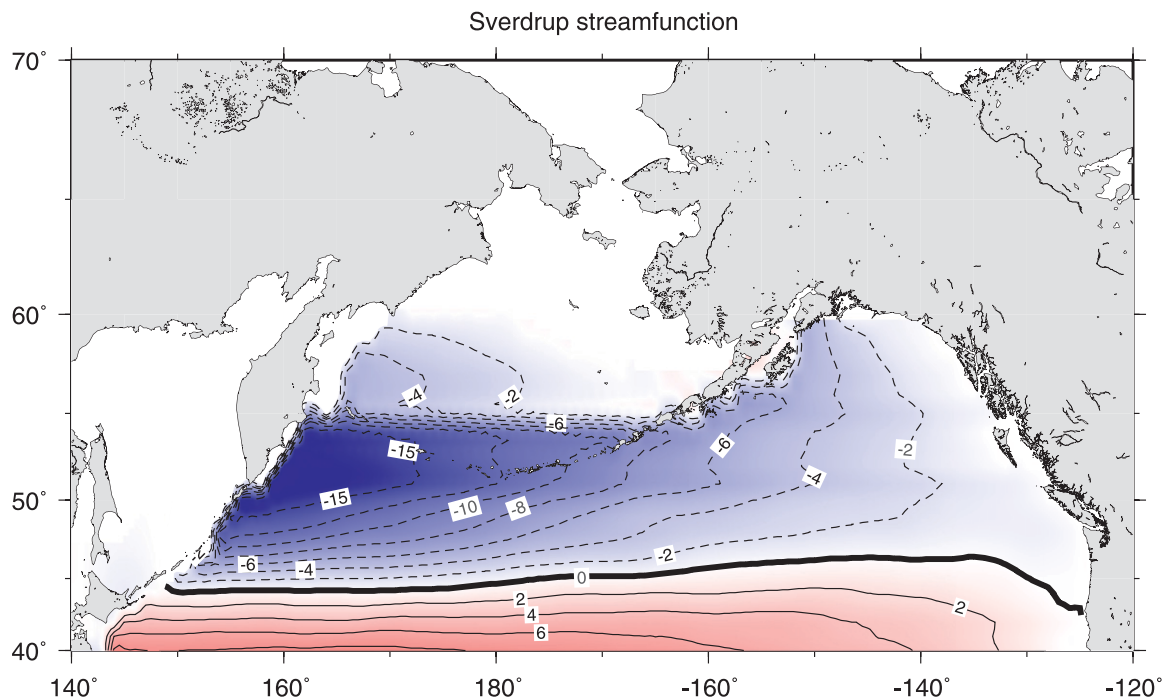


FIG. 17. Sverdrup circulation of the North Pacific using ERS winds (1991–2000) and Godfrey’s (1989) Island Rule.

boundary is the Alaska Peninsula/Aleutian Island arc), and the latitudes are comparable. As shown above, the wind stress curl in the Pacific is vastly diminished in the summer, yet the two gyres are present year-round. Furthermore, like the North Atlantic, the Pacific gyres seem to have a small seasonal cycle. According to Spall and Pickart (2003), a measure of the relative strength of the seasonal amplitude versus the mean circulation is given by the ratio of the distance that a baroclinic Rossby wave propagates in a year to the zonal length scale of the forcing. Using a baroclinic wave speed of 0.8 cm s^{-1} (Qiu 2002) and a forcing width scale of 1000 km (roughly the size of each wind stress curl signal in Fig. 15), this implies a seasonal amplitude for the North Pacific gyres of $O(25\%)$ of the mean. This is consistent with (though somewhat larger than) the observations noted above, which are themselves uncertain. This result also helps to explain the discrepancy noted by Musgrave et al. (1992) between the large predicted seasonal Sverdrup flow of the Alaska gyre, and the minimal signal they measured in the Alaskan Stream.

A final insight regarding the importance of the bimodal wind stress curl signal pertains to the Sverdrup circulation of the North Pacific. Using wind data from ship reports over a 15-yr period, Kutsuwada (1982) computed the mean Sverdrup flow that was greater than 20 Sv. Because of the substantial spatial averaging, however, the pattern shows little detail. We computed the Sverdrup circulation using Godfrey’s (1989) Island Rule applied

to ERS winds. A monthly average annual cycle of wind stress was constructed from the 9.5 yr of data (1991–2000), and the mean of this cycle was used for the curl and subsequent transport calculation. The Godfrey (1989) Island Rule is a generalized Sverdrup streamfunction that determines the total transport between an island and the coast to its east (and thus the western boundary transport along the island’s coast), using the interior wind-driven Sverdrup flow plus the assumption of cross-stream geostrophy in western boundary currents (see also Wajsowicz 1993 and Pedlosky et al. 1997).

The island rule streamfunction field so computed shows northward flow in the Gulf of Alaska corresponding to the enhanced wind stress curl there, as well as the northward flow in the west associated with the second region of enhanced curl near Kamchatka (Fig. 17). Of course, this is a flat-bottom calculation based on classic Sverdrup dynamics, and hence it can only tell part of the story. All the return flow along the Alaska Peninsula (which is a streamline) feeds a zonal jet through the first opening in the Aleutian Island arc (Unimak Pass), and there are no closed streamlines associated with the Alaska gyre. In Spall and Pickart’s (2003) North Atlantic model, a recirculation was established coincident with the enhanced curl east of Greenland. This was the result of dissipation due to the close proximity of the northern and southern limbs of the broad basinwide cyclonic flow near the apex of southern

Greenland. It is possible that a similar effect happens in the North Pacific because of the southward-protruding Alaska Peninsula–Aleutian Island arc, especially in light of the enhanced eddy activity reported near the apex of the arc (Cokelet et al. 1996). This idea warrants further study.

Acknowledgments. This work was carried out while RP was on sabbatical at the University of Alaska, Fairbanks (UAF) and the International Arctic Research Center (IARC). RP acknowledges the generous support provided by D. Wiesenburg (UAF) and S. Akasofu (IARC). RP is indebted to Tom Weingartner for making the visit possible and for many stimulating discussions. K. Våge helped with the QuikSCAT and NCEP data analysis, S. Danielson provided various technical assistance, T. McKee aided in figure preparation, and R. Goldsmith provided programming support. The following funding sources are acknowledged: Office of Naval Research Grant N00014-02-1-0317 (RP); Natural Sciences and Engineering Research Council of Canada (GWKM); National Science Foundation Grant OCE-0623261 (AM); Natural Environmental Research Council Grant NE/C003365/1 (IR).

REFERENCES

- Anderson, J. R., and J. R. Gyakum, 1989: A diagnostic study of Pacific Basin circulation regimes as determined from extratropical cyclone tracks. *Mon. Wea. Rev.*, **117**, 2672–2686.
- Businger, S., 1987: The synoptic climatology of polar-low outbreaks over the Gulf of Alaska. *Tellus*, **39A**, 307–325.
- Cokelet, E. D., M. L. Schall, and D. M. Dougherty, 1996: ADCP-referenced geostrophic circulation in the Bering Sea Basin. *J. Phys. Oceanogr.*, **26**, 1113–1128.
- Curry, R. G., 2002: HydroBase 2: A database of hydrographic profiles and tools for climatological analysis. Woods Hole Oceanographic Institution Tech. Rep. 96-01, 81 pp.
- Davis, R., 1976: Predictability of sea surface temperature and sea level pressure anomalies over the North Pacific Ocean. *J. Phys. Oceanogr.*, **6**, 249–266.
- DeCosmo, J., K. B. Katsaros, S. D. Smith, R. J. Anderson, W. A. Oost, K. Bunke, and H. Chadwick, 1996: Air–sea exchange of water vapor and sensible heat: The Humidity Exchange over the Sea (HEXOS) results. *J. Geophys. Res.*, **101**, 12 001–12 016.
- Favorite, F., A. J. Dodimead, and K. Nasu, 1976: Oceanography of the subarctic Pacific region, 1962–72. *Bull. Int. North Pacific Fish. Comm.*, **33**, 1–187.
- Feldstein, S. B., 2003: Fundamental mechanisms of the growth and decay of the Pacific–North American teleconnection pattern. *Quart. J. Roy. Meteor. Soc.*, **108**, 775–796.
- Godfrey, J. S., 1989: A Sverdrup model of the depth-integrated flow for the World Ocean allowing for island circulations. *Geophys. Astrophys. Fluid Dyn.*, **45**, 89–112.
- Gyakum, J. R., J. R. Anderson, R. H. Grumm, and E. L. Gruner, 1989: North Pacific cold-season surface cyclone activity: 1975–1983. *Mon. Wea. Rev.*, **117**, 1141–1155.
- Hoskins, B. J., M. E. McIntyre, and A. W. Robertson, 1985: On the use and significance of isentropic potential vorticity maps. *Quart. J. Roy. Meteor. Soc.*, **111**, 877–946.
- Kono, T., and Y. Kawasaki, 1997: Results of CTD and mooring observations southeast of Hokkaido. 1. Annual velocity and transport variations in the Oyashio. *Bull. Hokkaido Natl. Fish. Res. Inst.*, **61**, 65–81.
- Kushnir, Y., W. A. Robinson, I. Blade, N. M. J. Hall, S. Peng, and R. Sutton, 2002: Atmospheric GCM response to extratropical SST anomalies: Synthesis and evaluation. *J. Climate*, **15**, 2233–2256.
- Kutsuwada, K., 1982: New computation of the wind stress over the North Pacific Ocean. *J. Oceanogr. Soc. Japan*, **38**, 159–171.
- Lavender, K. L., 2001: The general circulation and open-ocean deep convection in the Labrador Sea: A study using subsurface floats. Ph.D. Thesis, University of California, San Diego, Scripps Institution of Oceanography, 131 pp.
- , R. E. Davis, and W. B. Owens, 2000: Mid-depth recirculation observed in the interior Labrador and Irminger Seas by direct velocity measurements. *Nature*, **407**, 66–69.
- Loescher, K. A., G. S. Young, B. A. Colle, and N. S. Winstead, 2006: Climatology of barrier jets along the Alaskan coast. Part I: Spatial and temporal distributions. *Mon. Wea. Rev.*, **134**, 437–453.
- Macdonald, A. M., T. Suga, and R. G. Curry, 2001: An isopycnally averaged North Pacific climatology. *J. Atmos. Oceanic Technol.*, **18**, 394–420.
- Mantua, N. J., S. R. Hare, Y. Zhang, J. M. Wallace, and R. C. Francis, 1997: A Pacific interdecadal climate oscillation with impacts on salmon production. *Bull. Amer. Meteor. Soc.*, **78**, 1069–1079.
- Moore, G. W. K., and I. A. Renfrew, 2002: An assessment of the surface turbulent heat fluxes from the NCEP–NCAR reanalysis over the western boundary currents. *J. Climate*, **15**, 2020–2037.
- Musgrave, D. L., T. J. Weingartner, and T. C. Royer, 1992: Circulation and hydrography in the northwestern Gulf of Alaska. *Deep-Sea Res.*, **39**, 1499–1519.
- Overland, J. E., and R. T. Hiester, 1980: Development of a synoptic climatology for the northeast Gulf of Alaska. *J. Appl. Meteor.*, **19**, 1–14.
- , and C. H. Pease, 1982: Cyclone climatology of the Bering Sea and its relation to sea ice extent. *Mon. Wea. Rev.*, **110**, 5–13.
- , M. C. Spillane, H. E. Hurlburt, and A. J. Wallcraft, 1994: A numerical study of the circulation of the Bering Sea Basin and exchange with the North Pacific Ocean. *J. Phys. Oceanogr.*, **24**, 736–758.
- Panteleev, G. G., P. Stabeno, V. A. Luchin, D. A. Nechaev, and M. Ikeda, 2006: Summer transport estimates of the Kamchatka Current derived as a variational inverse of hydrophysical and surface drifter data. *Geophys. Res. Lett.*, **33**, L09609, doi:10.1029/2005GL024974.
- Pedlosky, J., L. J. Pratt, M. A. Spall, and K. R. Helfrich, 1997: Circulation around islands and ridges. *J. Mar. Res.*, **30**, 1199–1251.
- Pickart, R. S., M. A. Spall, M. H. Ribergaard, G. W. K. Moore, and R. F. Milliff, 2003: Deep convection in the Irminger Sea forced by the Greenland tip jet. *Nature*, **424**, 152–156.
- Plakhotnik, A. F., 1964: Hydrological description of the Gulf of Alaska. Part II. *Soviet Fisheries Investigations in the Northeast Pacific*, P. A. Moiseev, Ed., Russian Federal Research Institute of Fishery and Oceanography (VNIRO), 289 pp.
- Qiu, B., 2002: Large-scale variability in the midlatitude subtropical and subpolar North Pacific Ocean: Observations and causes. *J. Phys. Oceanogr.*, **32**, 353–375.

- Reed, R. K., R. D. Muench, and J. D. Schumacher, 1980: On baroclinic transport of the Alaskan Stream near Kodiak Island. *Deep-Sea Res.*, **27**, 509–523.
- Renfrew, I. A., G. W. K. Moore, P. S. Guest, and K. Bumke, 2002: A comparison of surface-layer heat flux and surface momentum flux observations over the Labrador Sea with ECMWF analyses and NCEP reanalyses. *J. Phys. Oceanogr.*, **32**, 383–400.
- Rodionov, S. N., J. E. Overland, and N. A. Bond, 2005a: Spatial and temporal variability of the Aleutian climate. *Fish. Oceanogr.*, **14**, 3–21.
- , —, and —, 2005b: The Aleutian low and winter climatic conditions in the Bering Sea. Part I: Classification. *J. Climate*, **18**, 160–177.
- Roden, G., 1970: Aspects of the mid-Pacific transition zone. *J. Geophys. Res.*, **75**, 1097–1109.
- Royer, T. C., 1981: Baroclinic transport in the Gulf of Alaska, Part I. Seasonal variations of the Alaska Current. *J. Mar. Res.*, **39**, 239–250.
- Sanders, F., and J. R. Gyakum, 1980: Synoptic–dynamic climatology of the “bomb.” *Mon. Wea. Rev.*, **108**, 1589–1606.
- Serreze, M. C., R. Carse, and R. Barry, 1997: Icelandic low cyclone activity: Climatological features, linkages with the NAO, and relationships with recent changes in the Northern Hemisphere circulation. *J. Climate*, **10**, 453–464.
- Smirnov, V. V., and G. W. K. Moore, 2001: Short-term and seasonal variability of the atmospheric water vapor transport through the Mackenzie River basin. *J. Hydrometeor.*, **2**, 441–452.
- Smith, S. D., 1988: Coefficients for sea surface wind stress, heat flux, and wind profiles as a function of wind speed and temperature. *J. Geophys. Res.*, **93**, 15 467–15 472.
- Spall, M. A., and R. S. Pickart, 2003: Wind-driven recirculations and exchange in the Labrador and Irminger Seas. *J. Phys. Oceanogr.*, **33**, 1829–1845.
- Stabeno, P. J., and R. K. Reed, 1992: A major circulation anomaly in the western Bering Sea. *Geophys. Res. Lett.*, **19**, 1671–1674.
- , J. D. Schumacher, and K. Ohtani, 1999: The physical oceanography of the Bering Sea. *Dynamics of the Bering Sea: A Summary of Physical, Chemical, and Biological Characteristics, and a Synopsis of Research on the Bering Sea*, T. R. Loughlin and K. Ohtani, Eds., University of Alaska Sea Grant AK-SG-99-03, North Pacific Marine Science Organization (PICES), 1–28.
- , D. G. Kachel, N. B. Kachel, and M. E. Sullivan, 2005: Observations from moorings in the Aleutian Passes: Temperature, salinity and transport. *Fish. Oceanogr.*, **14** (Suppl. 1), 39–54.
- Terada, K., and M. Hanzawa, 1984: Climate of the North Pacific Ocean. *Climates of the Oceans*, H. Van Loon, Ed., Vol. 15, *World Survey of Climatology*, Elsevier, 431–477.
- Thomson, R. E., 1972: On the Alaskan Stream. *J. Phys. Oceanogr.*, **2**, 363–371.
- Trenberth, K. E., and J. W. Hurrell, 1994: Decadal atmosphere–ocean variations in the Pacific. *Climate Dyn.*, **9**, 303–319.
- Uehara, K., H. Miyake, and M. Okazaki, 1997: Characteristics of the flows in the Oyashio area off Cape Erimo, Hokkaido, Japan. *J. Oceanogr.*, **53**, 93–103.
- , S.-I. Ito, H. Miyake, I. Yasuda, Y. Shimizu, and T. Watanabe, 2004: Absolute volume transports of the Oyashio referred to moored current meter data crossing the OICE. *J. Oceanogr.*, **60**, 397–409.
- Våge, K., R. S. Pickart, G. W. K. Moore, and M. H. Ribergaard, 2008: Winter mixed layer development in the central Irminger Sea: The effect of strong, intermittent wind events. *J. Phys. Oceanogr.*, **38**, 541–565.
- Wajsowicz, R. C., 1993: The circulation of the depth-integrated flow around an island with application to the Indonesian Throughflow. *J. Phys. Oceanogr.*, **23**, 1470–1484.
- Wallace, J. M., and D. S. Gutzler, 1981: Teleconnections of the geopotential height field during the Northern Hemisphere winter. *Mon. Wea. Rev.*, **109**, 784–812.
- Warren, B. A., and W. B. Owens, 1988: Deep currents in the central subarctic Pacific Ocean. *J. Phys. Oceanogr.*, **18**, 529–551.
- Wentz, F., D. Smith, C. Mears, and C. Gentemann, 2001: Advanced algorithms for QuikScat and SeaWinds/AMSR. *Proc. Int. Geosci. Remote Sens. Symp. (IGARSS'01)*, Sydney, NSW, Australia, IEEE, 1079–1081.
- White, W. B., and T. P. Barnett, 1972: A servomechanism in the ocean/atmosphere system of the midlatitude North Pacific Ocean. *J. Phys. Oceanogr.*, **2**, 372–381.
- Wilson, J. G., and J. E. Overland, 1986: Meteorology. *The Gulf of Alaska, Physical Environment and Biological Resources*, D. W. Hood and S. T. Zimmerman, Eds., Alaska Office, Ocean Assessments Division, National Oceanic and Atmospheric Administration, U.S. Department of Commerce, 655 pp.
- Wise, J. L., A. L. Comisky, and R. Becker Jr., 1981: Storm surge climatology and forecasting in Alaska. Arctic Environmental Information and Data Center, University of Alaska, Anchorage, 53 pp.
- Zhang, X., J. E. Walsh, J. Zhang, U. S. Bhatt, and M. Ikeda, 2004: Climatology and interannual variability of Arctic cyclone activity: 1948–2002. *J. Climate*, **17**, 2300–2317.